

# OTFS: A New Modulation Scheme for 5G and Beyond

**NCC'2020 Tutorial  
IIT Kharagpur**

**A. Chockalingam  
Department of ECE, IISc**

Special thanks to  
M. K. Ramachandran, G. D. Surabhi, Rosemary Augustine, Prof. Emanuele Viterbo

**21 February 2020**

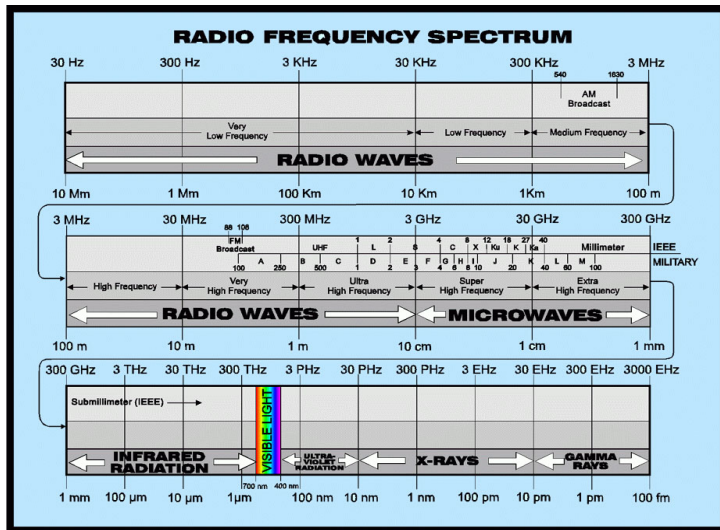


# Outline I

- 1 Some background
- 2 High-mobility requirement in 5G
- 3 OTFS modulation
- 4 Performance of OTFS
  - Diversity in OTFS
  - MIMO-OTFS
  - Space-time coded OTFS
  - PAPR of OTFS
  - Channel estimation in OTFS
  - Multiuser OTFS (OTFS-MA)
  - Effect of phase noise on OTFS
- 5 Conclusions

# Some background

# Wireless spectrum



Source: Internet



# Some wireless terminologies

# Some wireless terminologies

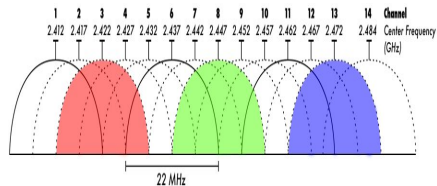
- Carrier frequency (Hertz; Hz)

# Some wireless terminologies

- Carrier frequency (Hertz; Hz)
- Bandwidth,  $W$  (Hz)

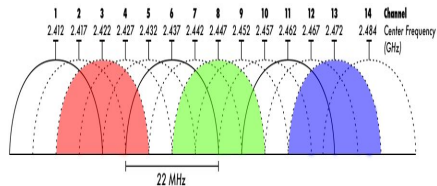
# Some wireless terminologies

- Carrier frequency (Hertz; Hz)
- Bandwidth,  $W$  (Hz)



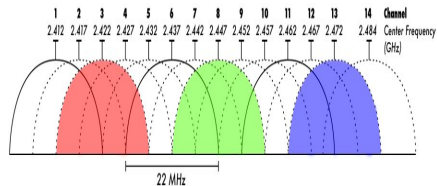
# Some wireless terminologies

- Carrier frequency (Hertz; **Hz**)
- Bandwidth,  $W$  (Hz)
- Data rate (bits per second; **bps**)



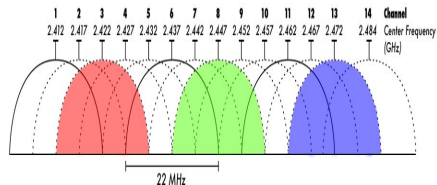
# Some wireless terminologies

- Carrier frequency (Hertz; Hz)
- Bandwidth,  $W$  (Hz)
- Data rate (bits per second; bps)
- Spectral efficiency (bps per Hz; bps/Hz)



# Some wireless terminologies

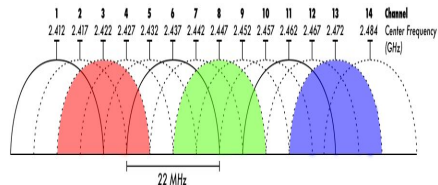
- Carrier frequency (Hertz; **Hz**)
- Bandwidth,  $W$  (Hz)
- Data rate (bits per second; **bps**)
- Spectral efficiency (bps per Hz; **bps/Hz**)
- Signaling interval,  $T_s = \frac{1}{W}$  (**sec**)



# Some wireless terminologies

- Carrier frequency (Hertz; **Hz**)

- Bandwidth,  $W$  (Hz)

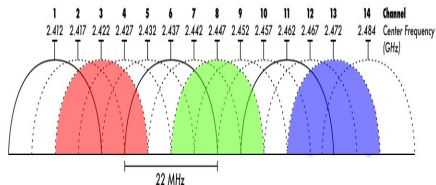


- Data rate (bits per second; **bps**)
- Spectral efficiency (bps per Hz; **bps/Hz**)
- Signaling interval,  $T_s = \frac{1}{W}$  (**sec**)
- Signal-to-noise ratio (SNR)



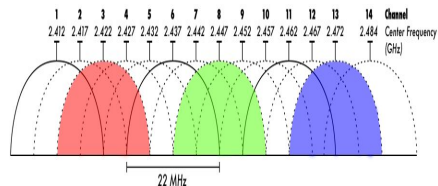
# Some wireless terminologies

- Carrier frequency (Hertz; **Hz**)
- Bandwidth,  $W$  (Hz)
- Data rate (bits per second; **bps**)
- Spectral efficiency (bps per Hz; **bps/Hz**)
- Signaling interval,  $T_s = \frac{1}{W}$  (**sec**)
- Signal-to-noise ratio (SNR)
- Channel capacity (**bps**)



# Some wireless terminologies

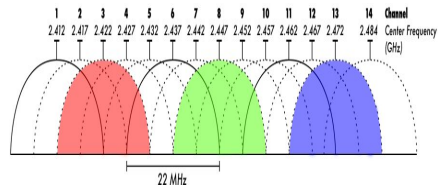
- Carrier frequency (Hertz; **Hz**)
- Bandwidth,  $W$  (Hz)
- Data rate (bits per second; **bps**)
- Spectral efficiency (bps per Hz; **bps/Hz**)
- Signaling interval,  $T_s = \frac{1}{W}$  (**sec**)
- Signal-to-noise ratio (SNR)
- Channel capacity (**bps**)
- Probability of bit error



# Some wireless terminologies

- Carrier frequency (Hertz; Hz)

- Bandwidth,  $W$  (Hz)



- Data rate (bits per second; bps)

- Spectral efficiency (bps per Hz; bps/Hz)

- Signaling interval,  $T_s = \frac{1}{W}$  (sec)

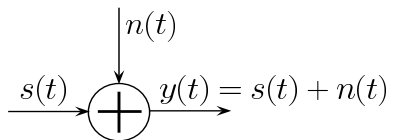
- Signal-to-noise ratio (SNR)

- Channel capacity (bps)

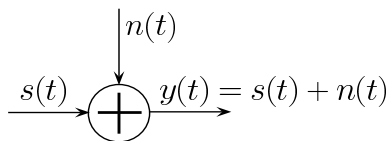
- Probability of bit error

- Multipath fading

# AWGN channel

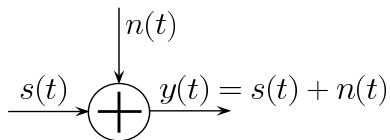


# AWGN channel



- e.g., satellite channel

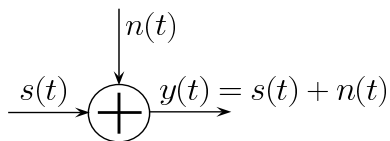
# AWGN channel



- e.g., satellite channel

Channel	Error Probability ( $P_e$ )	Capacity ( $C$ ), bps
AWGN	$P_e \propto e^{-SNR}$	$C = W \log(1 + SNR)$

# AWGN channel



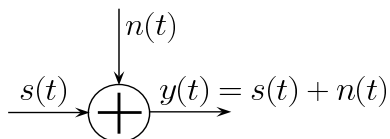
- e.g., satellite channel

Channel	Error Probability ( $P_e$ )	Capacity ( $C$ ), bps
AWGN	$P_e \propto e^{-SNR}$	$C = W \log(1 + SNR)$

- Prob. of error falls exponentially with SNR



# AWGN channel



- e.g., satellite channel

Channel	Error Probability ( $P_e$ )	Capacity ( $C$ ), bps
AWGN	$P_e \propto e^{-SNR}$	$C = W \log(1 + SNR)$

- Prob. of error falls exponentially with SNR ☺

- Capacity grows with SNR (but only logarithmically with SNR) ☹



# Multipath fading

- Fading channel characterization

- Fading channel characterization
  - Variation in frequency-domain
    - Max. Delay spread ( $\tau_{max}$ )
    - Coherence bandwidth ( $W_{coh}$ )

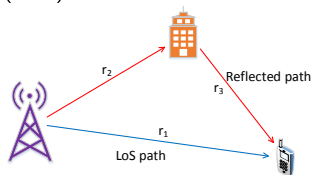
- Fading channel characterization
  - Variation in frequency-domain
    - Max. Delay spread ( $\tau_{max}$ )
    - Coherence bandwidth ( $W_{coh}$ )
  - Variation in time-domain
    - Max. Doppler spread ( $\nu_{max}$ )
    - Coherence time ( $T_{coh}$ )

# Multipath fading

- Variation in frequency-domain
  - Max. Delay spread ( $\tau_{max}$ ) and coherence bandwidth ( $W_{coh}$ )

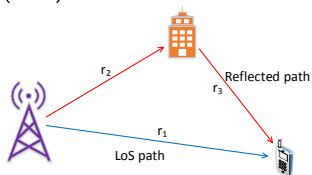
# Multipath fading

- Variation in frequency-domain
  - Max. Delay spread ( $\tau_{max}$ ) and coherence bandwidth ( $W_{coh}$ )



# Multipath fading

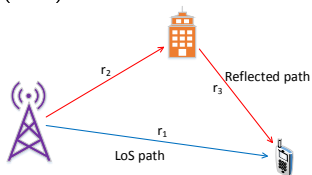
- Variation in frequency-domain
  - Max. Delay spread ( $\tau_{max}$ ) and coherence bandwidth ( $W_{coh}$ )



- Delay of LoS path:  $\tau_1 = r_1/c$ .

# Multipath fading

- Variation in frequency-domain
  - Max. Delay spread ( $\tau_{max}$ ) and coherence bandwidth ( $W_{coh}$ )

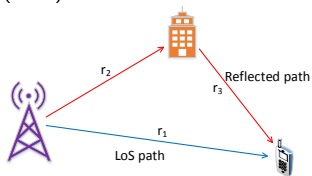


- Delay of LoS path:  $\tau_1 = r_1/c$ .    Delay of reflected path:  $\tau_2 = (r_2 + r_3)/c$



# Multipath fading

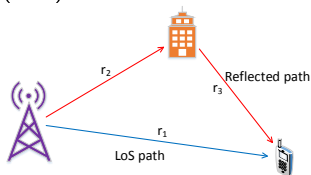
- Variation in frequency-domain
  - Max. Delay spread ( $\tau_{max}$ ) and coherence bandwidth ( $W_{coh}$ )



- Delay of LoS path:  $\tau_1 = r_1/c$ .      Delay of reflected path:  $\tau_2 = (r_2 + r_3)/c$
- Delay spread:  $\tau_2 - \tau_1$ .

# Multipath fading

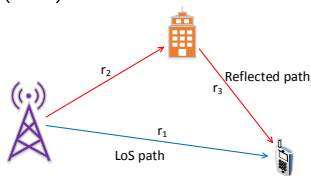
- Variation in frequency-domain
  - Max. Delay spread ( $\tau_{max}$ ) and coherence bandwidth ( $W_{coh}$ )



- Delay of LoS path:  $\tau_1 = r_1/c$ . Delay of reflected path:  $\tau_2 = (r_2 + r_3)/c$
- Delay spread:  $\tau_2 - \tau_1$ .  $\tau_{max} = \max_{i,j} |\tau_i - \tau_j|$

# Multipath fading

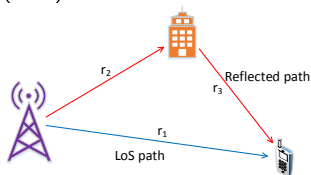
- Variation in frequency-domain
  - Max. Delay spread ( $\tau_{max}$ ) and coherence bandwidth ( $W_{coh}$ )



- Delay of LoS path:  $\tau_1 = r_1/c$ . Delay of reflected path:  $\tau_2 = (r_2 + r_3)/c$
- Delay spread:  $\tau_2 - \tau_1$ .  $\tau_{max} = \max_{i,j} |\tau_i - \tau_j|$
- $W_{coh} \propto \tau_{max}^{-1}$

# Multipath fading

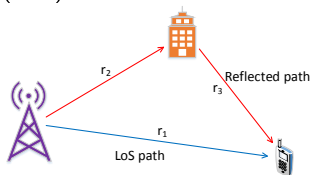
- Variation in frequency-domain
  - Max. Delay spread ( $\tau_{max}$ ) and coherence bandwidth ( $W_{coh}$ )



- Delay of LoS path:  $\tau_1 = r_1/c$ . Delay of reflected path:  $\tau_2 = (r_2 + r_3)/c$
- Delay spread:  $\tau_2 - \tau_1$ .  $\tau_{max} = \max_{i,j} |\tau_i - \tau_j|$
- $W_{coh} \propto \tau_{max}^{-1}$
- Frequency-flat fading: Coherence BW > Signaling BW ( $W_{coh} > W$ )

# Multipath fading

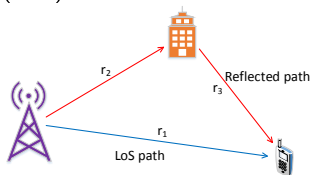
- Variation in frequency-domain
  - Max. Delay spread ( $\tau_{max}$ ) and coherence bandwidth ( $W_{coh}$ )



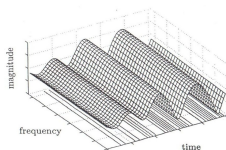
- Delay of LoS path:  $\tau_1 = r_1/c$ . Delay of reflected path:  $\tau_2 = (r_2 + r_3)/c$
- Delay spread:  $\tau_2 - \tau_1$ .  $\tau_{max} = \max_{i,j} |\tau_i - \tau_j|$
- $W_{coh} \propto \tau_{max}^{-1}$
- Frequency-flat fading: Coherence BW > Signaling BW ( $W_{coh} > W$ )
- Frequency-selective fading: Coherence BW < Signaling BW ( $W_{coh} < W$ )

# Multipath fading

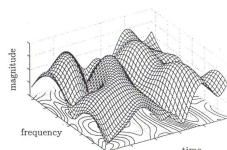
- Variation in frequency-domain
  - Max. Delay spread ( $\tau_{max}$ ) and coherence bandwidth ( $W_{coh}$ )



- Delay of LoS path:  $\tau_1 = r_1/c$ . Delay of reflected path:  $\tau_2 = (r_2 + r_3)/c$
- Delay spread:  $\tau_2 - \tau_1$ .  $\tau_{max} = \max_{i,j} |\tau_i - \tau_j|$
- $W_{coh} \propto \tau_{max}^{-1}$
- Frequency-flat fading: Coherence BW > Signaling BW ( $W_{coh} > W$ )
- Frequency-selective fading: Coherence BW < Signaling BW ( $W_{coh} < W$ )



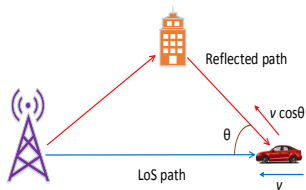
Frequency-flat fading.



Frequency-selective fading.

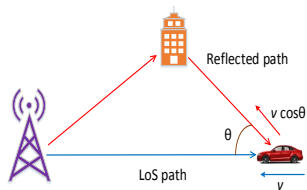
# Multipath fading

- Variation in time-domain
  - Max. Doppler spread ( $\nu_{max}$ ) and coherence time ( $T_{coh}$ )



# Multipath fading

- Variation in time-domain
  - Max. Doppler spread ( $\nu_{max}$ ) and coherence time ( $T_{coh}$ )

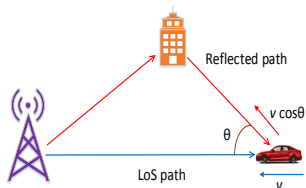


- Doppler shift of LoS path:  $\nu_1 = \frac{v}{\lambda} = f_c \frac{v}{c}$



# Multipath fading

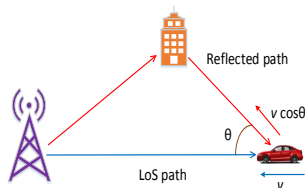
- Variation in time-domain
  - Max. Doppler spread ( $\nu_{max}$ ) and coherence time ( $T_{coh}$ )



- Doppler shift of LoS path:  $\nu_1 = \frac{v}{\lambda} = f_c \frac{v}{c}$
- Doppler shift of reflected path:  $\nu_2 = f_c \frac{v \cos \theta}{c}$

# Multipath fading

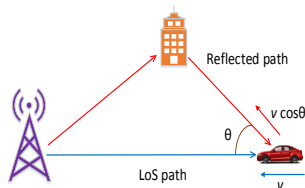
- Variation in time-domain
  - Max. Doppler spread ( $\nu_{max}$ ) and coherence time ( $T_{coh}$ )



- Doppler shift of LoS path:  $\nu_1 = \frac{v}{\lambda} = f_c \frac{v}{c}$
- Doppler shift of reflected path:  $\nu_2 = f_c \frac{v \cos \theta}{c}$
- Doppler spread:  $\nu_2 - \nu_1$

# Multipath fading

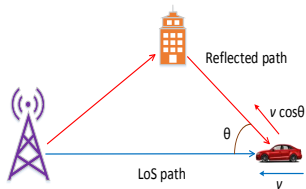
- Variation in time-domain
  - Max. Doppler spread ( $\nu_{max}$ ) and coherence time ( $T_{coh}$ )



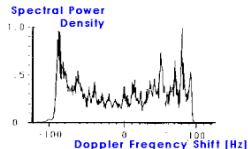
- Doppler shift of LoS path:  $\nu_1 = \frac{v}{\lambda} = f_c \frac{v}{c}$
- Doppler shift of reflected path:  $\nu_2 = f_c \frac{v \cos \theta}{c}$
- Doppler spread:  $\nu_2 - \nu_1$      $\nu_{max} = \max_{i,j} |\nu_i - \nu_j|$

# Multipath fading

- Variation in time-domain
  - Max. Doppler spread ( $\nu_{max}$ ) and coherence time ( $T_{coh}$ )

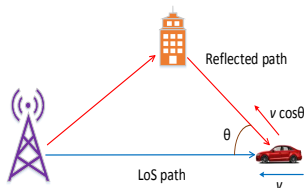


- Doppler shift of LoS path:  $\nu_1 = \frac{v}{\lambda} = f_c \frac{v}{c}$
- Doppler shift of reflected path:  $\nu_2 = f_c \frac{v \cos \theta}{c}$
- Doppler spread:  $\nu_2 - \nu_1$      $\nu_{max} = \max_{i,j} |\nu_i - \nu_j|$

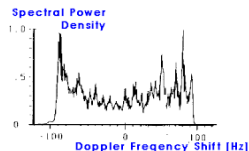


# Multipath fading

- Variation in time-domain
  - Max. Doppler spread ( $\nu_{max}$ ) and coherence time ( $T_{coh}$ )

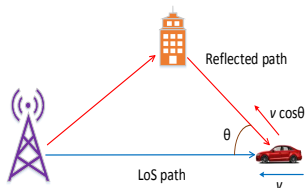


- Doppler shift of LoS path:  $\nu_1 = \frac{v}{\lambda} = f_c \frac{v}{c}$
- Doppler shift of reflected path:  $\nu_2 = f_c \frac{v \cos \theta}{c}$
- Doppler spread:  $\nu_2 - \nu_1$      $\nu_{max} = \max_{i,j} |\nu_i - \nu_j|$
  
- $T_{coh} \propto \nu_{max}^{-1}$

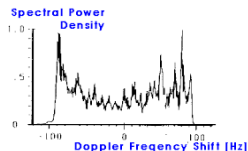


# Multipath fading

- Variation in time-domain
  - Max. Doppler spread ( $\nu_{max}$ ) and coherence time ( $T_{coh}$ )



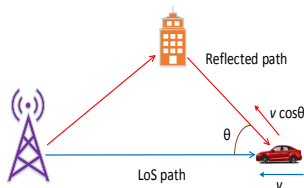
- Doppler shift of LoS path:  $\nu_1 = \frac{v}{\lambda} = f_c \frac{v}{c}$
- Doppler shift of reflected path:  $\nu_2 = f_c \frac{v \cos \theta}{c}$
- Doppler spread:  $\nu_2 - \nu_1$      $\nu_{max} = \max_{i,j} |\nu_i - \nu_j|$



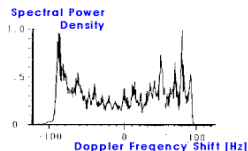
- $T_{coh} \propto \nu_{max}^{-1}$
- Slow fading: Coherence time > signaling interval ( $T_{coh} > T_s$ )

# Multipath fading

- Variation in time-domain
  - Max. Doppler spread ( $\nu_{max}$ ) and coherence time ( $T_{coh}$ )

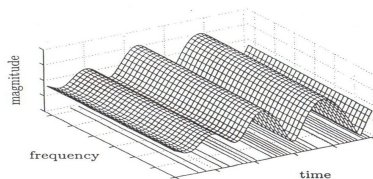
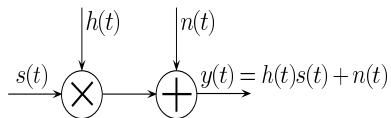


- Doppler shift of LoS path:  $\nu_1 = \frac{v}{\lambda} = f_c \frac{v}{c}$
- Doppler shift of reflected path:  $\nu_2 = f_c \frac{v \cos \theta}{c}$
- Doppler spread:  $\nu_2 - \nu_1$       $\nu_{max} = \max_{i,j} |\nu_i - \nu_j|$



- $T_{coh} \propto \nu_{max}^{-1}$
- Slow fading: Coherence time > signaling interval ( $T_{coh} > T_s$ )
- Fast fading: Coherence time < signaling interval ( $T_{coh} < T_s$ )

# Fading channel



Frequency-flat fading.

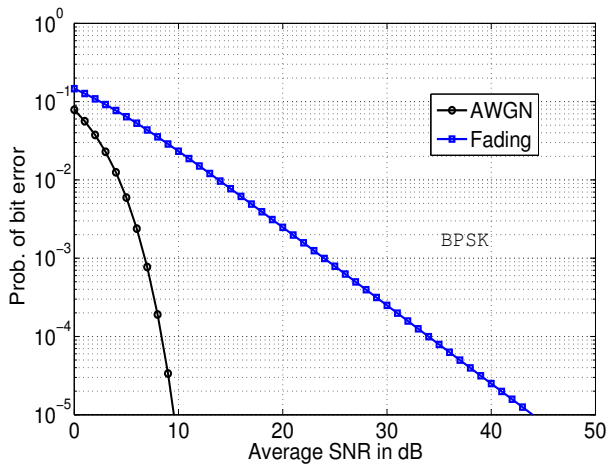
- e.g., mobile radio channel

Channel	Error Probability ( $P_e$ )	Capacity ( $C$ ), bps
Fading	$P_e \propto SNR^{-1}$	$C = W \log(1 + SNR)$

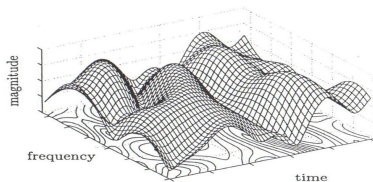
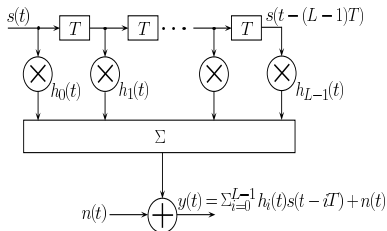
- Prob. of error falls only linearly with SNR ☹️



# Prob. of bit error performance



# ISI channel



Frequency-selective fading.

- e.g., mobile radio channel

Channel	Error Probability ( $P_e$ )	Capacity ( $C$ ), bps
ISI	$P_e \propto SNR^{-L}$	$C = W \log(1 + SNR)$

- Causes **inter-symbol interference (ISI)** ☹️
- If rx. signal is properly processed (equalization)
  - prob. of error **falls with  $L$ th power of SNR (multipath diversity)** 😊

# OFDM in ISI channels

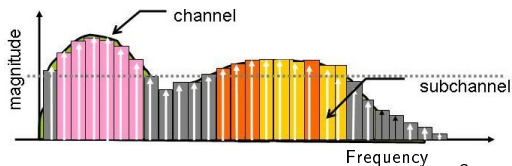
- Orthogonal Frequency Division Multiplexing (overcomes ISI issue)

# OFDM in ISI channels

- Orthogonal Frequency Division Multiplexing (overcomes ISI issue)
  - Converts frequency-selective channel to multiple ( $M$ ) frequency-flat channels

# OFDM in ISI channels

- Orthogonal Frequency Division Multiplexing (overcomes ISI issue)
  - Converts frequency-selective channel to multiple ( $M$ ) frequency-flat channels



Source: Internet

# OFDM in ISI channels

- Orthogonal Frequency Division Multiplexing (overcomes ISI issue)
  - Converts frequency-selective channel to multiple ( $M$ ) frequency-flat channels



Source: Internet

- Multiplexes  $M$  information symbols  $X(k)$ ,  $k = 0, \dots, M - 1$  on  $M$  subcarriers

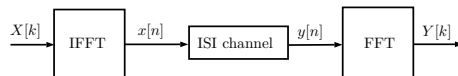
# OFDM in ISI channels

- Orthogonal Frequency Division Multiplexing (overcomes ISI issue)
  - Converts frequency-selective channel to multiple ( $M$ ) frequency-flat channels



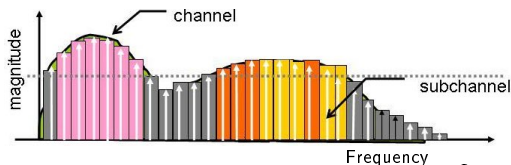
Source: Internet

- Multiplexes  $M$  information symbols  $X(k)$ ,  $k = 0, \dots, M - 1$  on  $M$  subcarriers



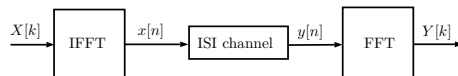
# OFDM in ISI channels

- Orthogonal Frequency Division Multiplexing (overcomes ISI issue)
  - Converts frequency-selective channel to multiple ( $M$ ) frequency-flat channels



Source: Internet

- Multiplexes  $M$  information symbols  $X(k)$ ,  $k = 0, \dots, M-1$  on  $M$  subcarriers

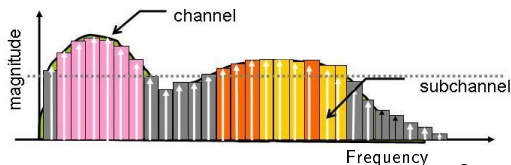


- Tx:  $x(n) = \frac{1}{\sqrt{M}} \sum_{k=0}^{M-1} X(k) e^{j2\pi kn/M}$ ,  $n = 0, 1, \dots, M-1$



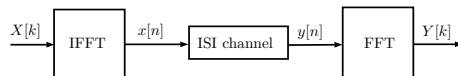
# OFDM in ISI channels

- Orthogonal Frequency Division Multiplexing (overcomes ISI issue)
  - Converts frequency-selective channel to multiple ( $M$ ) frequency-flat channels



Source: Internet

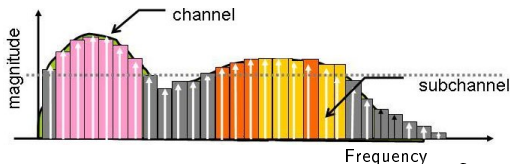
- Multiplexes  $M$  information symbols  $X(k)$ ,  $k = 0, \dots, M - 1$  on  $M$  subcarriers



- Tx:  $x(n) = \frac{1}{\sqrt{M}} \sum_{k=0}^{M-1} X(k) e^{j2\pi kn/M}$ ,  $n = 0, 1, \dots, M - 1$
- Rx:  $Y(k) = \frac{1}{\sqrt{M}} \sum_{n=0}^{M-1} y(n) e^{-j2\pi kn/M}$ ,  $k = 0, 1, \dots, M - 1$

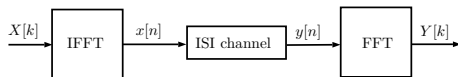
# OFDM in ISI channels

- Orthogonal Frequency Division Multiplexing (overcomes ISI issue)
  - Converts frequency-selective channel to multiple ( $M$ ) frequency-flat channels



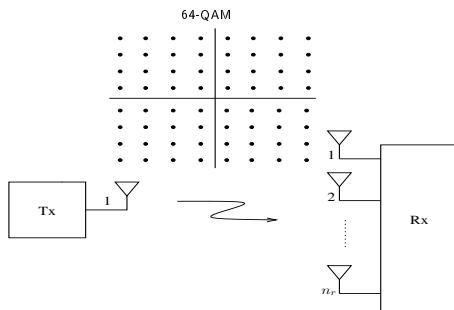
Source: Internet

- Multiplexes  $M$  information symbols  $X(k)$ ,  $k = 0, \dots, M-1$  on  $M$  subcarriers



- Tx:  $x(n) = \frac{1}{\sqrt{M}} \sum_{k=0}^{M-1} X(k) e^{j2\pi kn/M}$ ,  $n = 0, 1, \dots, M-1$
- Rx:  $Y(k) = \frac{1}{\sqrt{M}} \sum_{n=0}^{M-1} y(n) e^{-j2\pi kn/M}$ ,  $k = 0, 1, \dots, M-1$
- Renders the ISI channel to a multiplicative channel,  $Y(k) = H(k)X(k) + N(k)$

# SIMO channel

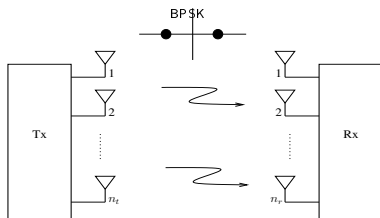


- e.g., mobile radio channel

Channel	Error Probability ( $P_e$ )	Capacity ( $C$ ), bps
SIMO	$P_e \propto SNR^{-n_r}$	$C = W \log(1 + SNR)$

- Prob. of error falls with  $n_r$ th power of SNR (receive diversity) 😊

# MIMO channel

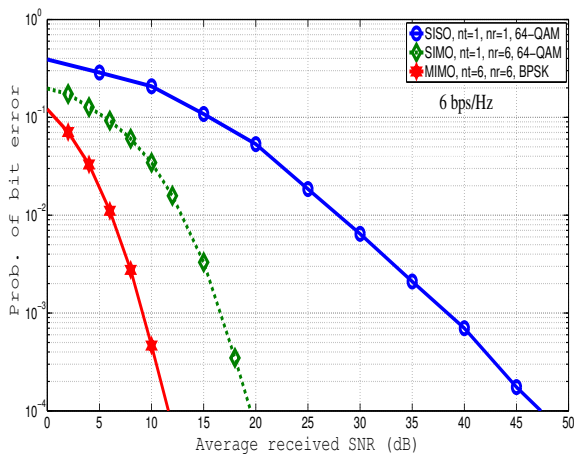


- e.g., mobile radio channel  $\mathbf{y} = \mathbf{H}\mathbf{x} + \mathbf{n}$

Channel	Error Probability ( $P_e$ )	Capacity ( $C$ ), bps
MIMO	$P_e \propto SNR^{-n_t n_r}$	$C = \min(n_t, n_r) W \log(1 + SNR)$

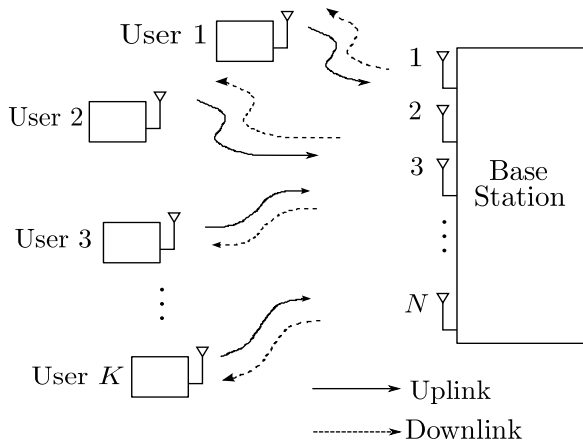
- Prob. of error falls with  $n_t n_r$ th power of SNR (tx & rx diversity) 😊
- Capacity grows linearly with  $n_t, n_r$  😊
- Large  $n_t, n_r \implies$  large capacity/diversity gains (massive MIMO in 5G)
- MIMO signal detection problem:  $\hat{\mathbf{x}} = \arg \max_{\mathbf{x} \in \mathbb{A}^{n_t}} \|\mathbf{y} - \mathbf{H}\mathbf{x}\|^2$

# Prob. of bit error performance



- MIMO
  - spectrally efficient, reliable, power efficient

# Multuser communication



# Cellular wireless evolution

Generation	Frequency band	PHY features	Data rate	Spectral Eff. (bps/Hz)
1G	850 MHz	FDMA, FM	N/A	N/A
2G	900 MHz, 1.8 GHz	TDMA/CDMA, GMSK/QPSK, FEC, PC	10 Kbps	< 1
3G	1.8–2.5 GHz	CDMA, QAM	1–40 Mbps	1–8
4G	2–8 GHz	OFDMA, SC-FDMA QAM, MIMO-OFDM	100–600 Mbps	15
5G	1–6 GHz mm wave (26–28 GHz) < 1 GHz (massive IoT) visible light?	massive MIMO beamforming D2D, Full duplex, NOMA LDPC and Polar codes OFDM & variants (adapted to extremes?)	multi-Gbps	several tens

- Waveform design is the major change between the generations

# High-mobility requirement in 5G



- ① **Enhanced mobile broadband (eMBB)** [2020-2021] (user focus)
  - High data rates (multi-gigabits per sec)
  - High spectral efficiency (tens of bps/Hz)
  - High capacity (10 Tbps per Km<sup>2</sup>)
  - **High user mobility?**

- 1 **Enhanced mobile broadband (eMBB)** [2020-2021] (user focus)
  - High data rates (multi-gigabits per sec)
  - High spectral efficiency (tens of bps/Hz)
  - High capacity (10 Tbps per Km<sup>2</sup>)
  - High user mobility?
- 2 **Massive machine type communications (mMTC)** [2021-2022] (device focus)
  - Massive Internet of Things
  - High density (1 million nodes per Km<sup>2</sup>)
  - Ultra-low energy (10 years+ battery life)
  - Deep coverage (reach challenging locations)

- 1 **Enhanced mobile broadband (eMBB)** [2020-2021] (user focus)
  - High data rates (multi-gigabits per sec)
  - High spectral efficiency (tens of bps/Hz)
  - High capacity (10 Tbps per Km<sup>2</sup>)
  - High user mobility?
- 2 **Massive machine type communications (mMTC)** [2021-2022] (device focus)
  - Massive Internet of Things
  - High density (1 million nodes per Km<sup>2</sup>)
  - Ultra-low energy (10 years+ battery life)
  - Deep coverage (reach challenging locations)
- 3 **Ultra-reliable and low-latency communications (uRLLC)** [2024-2025]
  - Mission-critical services
  - Ultra-low latency (< 1 msec end-to-end latency)
  - Ultra-high reliability (< 1 out of 100 million packets lost)
  - Strong security (health/financial/government)

# High-mobility support

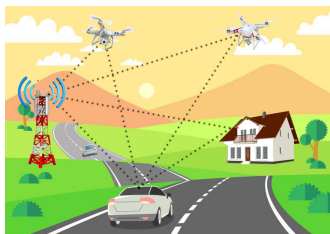
- Mobility support requirement
  - relative speed between the user and the network edge at which **consistent user experience must be ensured**
- Enhanced mobility support (~ 5-fold) compared to that in 4G
- **Mobility on demand**
  - ranging from very high mobility users (e.g., **users in bullet trains, airplanes**) to low mobility/stationary devices (e.g., **smart meters**)

Scenario	User experienced data rate	E2E latency	Mobility
Mobile BB in vehicles (cars, trains)	DL: 50 Mbps UL: 25 Mbps	10 msec	on demand up to 500 km/h
Airplane connectivity	DL: 15 Mbps UL: 7.5 Mbps	10 msec	on demand up to 1000 km/h

Scenario	Connection density	Traffic density
Mobile BB in vehicles (cars, trains)	2000/km <sup>2</sup> 500 active users/train, 4 trains or 1 active user/car, 2000 cars	DL: 100 Gbps/km <sup>2</sup> (25 Gbps/train, 50 Mbps/car) UL: 50 Gbps/km <sup>2</sup> (12.5 Gbps/train, 25 Mbps/car)
Airplane connectivity	80/plane 60 airplanes/18000 km <sup>2</sup>	DL: 1.2 Gbps/plane 600 Mbps/plane

(\*) "5G White Paper," ver 1.0, NGMN Alliance, Feb. 2015.

# High-Doppler wireless channels



- High Dopplers due to
  - High mobility (e.g., bullet trains)

Carrier frequency	UE speed	Doppler shift
4 GHz	27 kmph	100 Hz
	100 kmph	370.3 Hz
	500 kmph	1.851 KHz

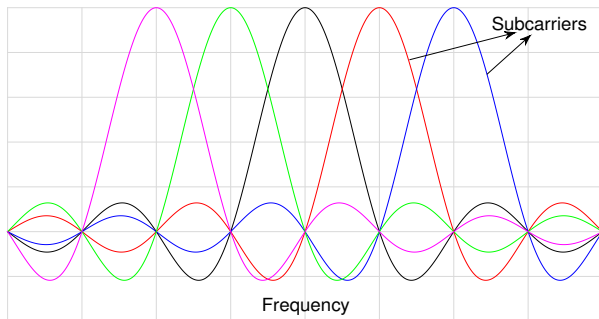
- High carrier frequencies (e.g., mmWave, 28 GHz)

Carrier frequency	UE speed	Doppler shift
28 GHz	27 kmph	700 Hz
	54 kmph	1.4 KHz

# OFDM (Modulation in 4G)

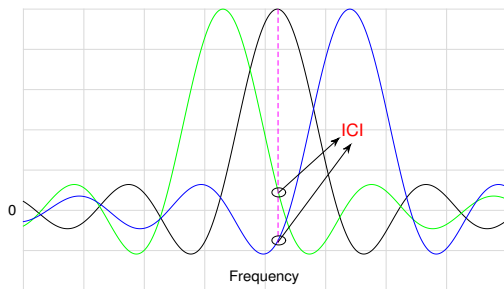
- OFDM

- Information is signaled in the frequency domain
- 1-D transform in frequency domain (IFFT/FFT)
- Orthogonality among the subcarriers is the key



# Effect of high Doppler in OFDM

- In presence of high Doppler, **subcarriers lose orthogonality**
- **This results in inter-carrier interference (ICI)**



- Causes severe degradation in bit error performance for high Dopplers (error floors)
- Channel estimation and equalization in high Doppler channels is difficult

# Time-frequency modulation

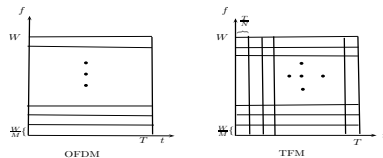


# Time-frequency modulation

- Bin both frequency and time axes (motivation: overcome the ICI effect)

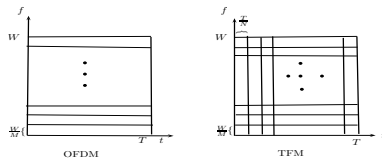
# Time-frequency modulation

- Bin both frequency and time axes (motivation: overcome the ICI effect)
- $M$  frequency bins and  $N$  time bins



# Time-frequency modulation

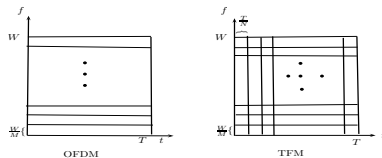
- Bin both frequency and time axes (motivation: overcome the ICI effect)
- $M$  frequency bins and  $N$  time bins



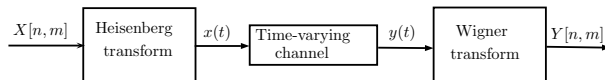
- Multiplex  $MN$  information symbols,  $X(n, m)$ , in the TF grid

# Time-frequency modulation

- Bin both frequency and time axes (motivation: overcome the ICI effect)
- $M$  frequency bins and  $N$  time bins

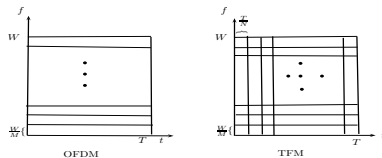


- Multiplex  $MN$  information symbols,  $X(n, m)$ , in the TF grid

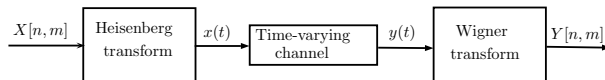


# Time-frequency modulation

- Bin both frequency and time axes (motivation: overcome the ICI effect)
- $M$  frequency bins and  $N$  time bins



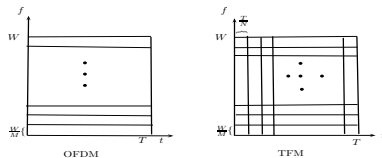
- Multiplex  $MN$  information symbols,  $X(n, m)$ , in the TF grid



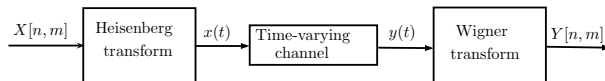
- Perform 2-D transform in the TF plane

# Time-frequency modulation

- Bin both frequency and time axes (motivation: overcome the ICI effect)
- $M$  frequency bins and  $N$  time bins



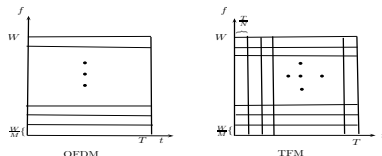
- Multiplex  $MN$  information symbols,  $X(n, m)$ , in the TF grid



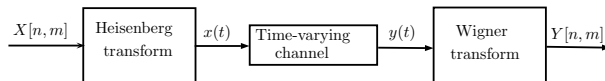
- Perform 2-D transform in the TF plane
- Tx:  $x(t) = \sum_{n=0}^{N-1} \sum_{m=0}^{M-1} X(n, m) g_t(t - nT) e^{j2\pi m \Delta f (t - nT)}$

# Time-frequency modulation

- Bin both frequency and time axes (motivation: overcome the ICI effect)
- $M$  frequency bins and  $N$  time bins



- Multiplex  $MN$  information symbols,  $X(n, m)$ , in the TF grid



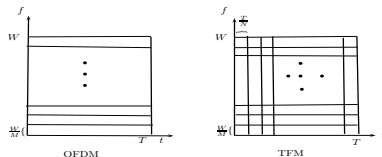
- Perform 2-D transform in the TF plane

- Tx: 
$$x(t) = \sum_{n=0}^{N-1} \sum_{m=0}^{M-1} X(n, m) g_t(t - nT) e^{j2\pi m \Delta f (t - nT)}$$

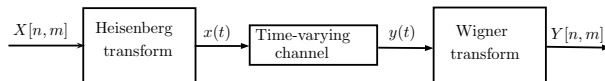
- Rx: 
$$Y(n, m) = A(t, f)|_{t=nT, f=m\Delta f}, A(t, f) = \int y(t') g_r^*(t' - t) e^{-j2\pi f(t' - t)} dt'$$

# Time-frequency modulation

- Bin both frequency and time axes (motivation: overcome the ICI effect)
- $M$  frequency bins and  $N$  time bins



- Multiplex  $MN$  information symbols,  $X(n, m)$ , in the TF grid



- Perform 2-D transform in the TF plane

- Tx: 
$$x(t) = \sum_{n=0}^{N-1} \sum_{m=0}^{M-1} X(n, m) g_t(t - nT) e^{j2\pi m \Delta f (t - nT)}$$

- Rx: 
$$Y(n, m) = A(t, f)|_{t=nT, f=m\Delta f}, A(t, f) = \int y(t') g_r^*(t' - t) e^{-j2\pi f(t' - t)} dt'$$

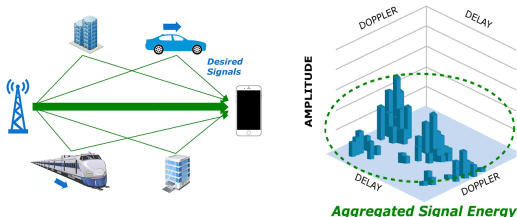
- Do not perform that well in high Dopplers



# OTFS modulation

# Orthogonal Time Frequency Space (OTFS) modulation\*

- A promising modulation scheme for doubly-selective channels
- Information is signaled in Delay-Doppler (DD) domain rather than in Time-Frequency (TF) domain



(\*) R. Hadani, S. Rakib, M. Tsatsanis, A. Monk, A. J. Goldsmith, A. F. Molisch, and R. Calderbank, "Orthogonal time frequency space modulation," in *Proc. IEEE WCNC*, San Francisco, CA, USA, March 2017.

# Why OTFS?

- OTFS Vs OFDM: A performance comparison

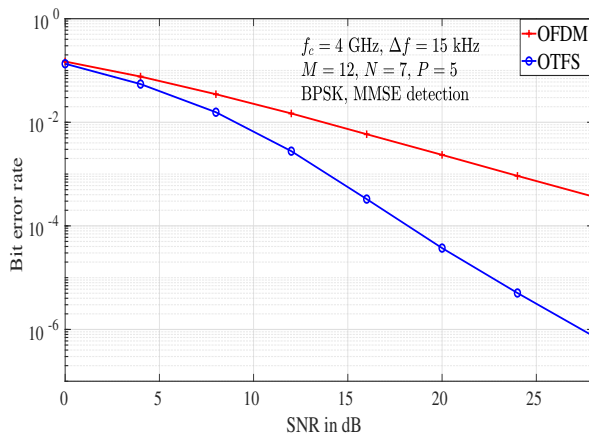
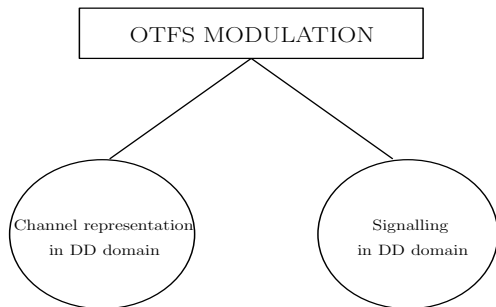


Figure : BER comparison of OTFS and OFDM systems with MMSE detection for  $f_c = 4$  GHz,  $\Delta f = 15$  KHz,  $M = 12$ ,  $N = 7$ ,  $P = 5$ ,  $\nu_{max} = 1.85$  KHz, BPSK.

# Key features of OTFS



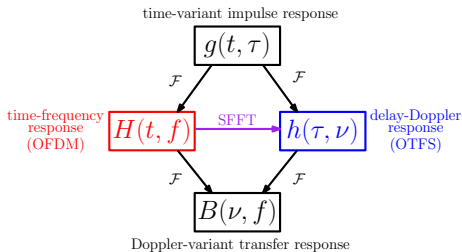
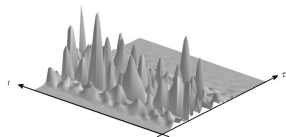
- Channel response in DD domain is invariant (for a larger observation time than in TF representation) and compact
- Each symbol experiences nearly constant channel gain
- Converts the multiplicative action of channel into a 2D convolution interaction with transmitted symbols

# Channel representation in DD domain

- Different representations can be used to model LTV multipath channel
  - in time ( $t$ ), frequency ( $f$ ), delay ( $\tau$ ), and Doppler ( $\nu$ ) variables
- Impulse response of a time-varying channel can be expressed as a function of
  - time-frequency  $H(t, f)$
  - time-delay  $g(t, \tau)$
  - delay-Doppler  $h(\tau, \nu)$

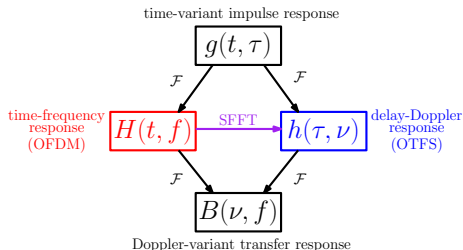
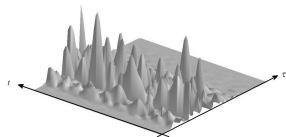
# Channel representation in DD domain

- Different representations can be used to model LTV multipath channel
  - in time ( $t$ ), frequency ( $f$ ), delay ( $\tau$ ), and Doppler ( $\nu$ ) variables
- Impulse response of a time-varying channel can be expressed as a function of
  - time-frequency  $H(t, f)$
  - time-delay  $g(t, \tau)$
  - delay-Doppler  $h(\tau, \nu)$



# Channel representation in DD domain

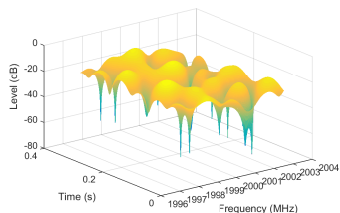
- Different representations can be used to model LTV multipath channel
  - in time ( $t$ ), frequency ( $f$ ), delay ( $\tau$ ), and Doppler ( $\nu$ ) variables
- Impulse response of a time-varying channel can be expressed as a function of
  - time-frequency  $H(t, f)$
  - time-delay  $g(t, \tau)$
  - delay-Doppler  $h(\tau, \nu)$



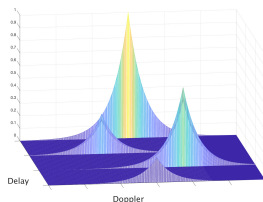
- In time-frequency  $H(t, f)$  and time-delay  $h(t, \tau)$  representations
  - channel coefficients vary with time at a rate that depends on mobility and carrier frequency

# Time-frequency and delay-Doppler responses

- DD domain impulse response  $h(\tau, \nu)$  is more compact
  - channel taps in DD representation correspond to a cluster of reflectors with specific delay and Doppler values
  - the delay and Doppler values depend on reflectors' relative distance and relative velocity, respectively, with the transmitter and receiver
  - relative velocity and distance remain roughly constant for at least a few msecs
  - Hence channel in DD domain appears time invariant for a longer duration
  - DD representation results in a sparse representation



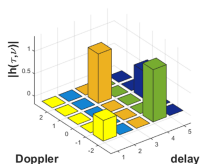
SFFT  
← ISFFT



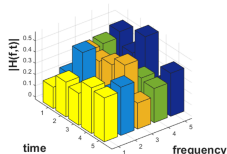
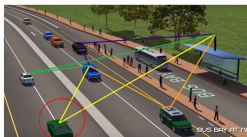
Channel in time-frequency  $H(t, f)$  and delay-Doppler  $h(\tau, \nu)$  domains



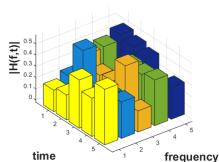
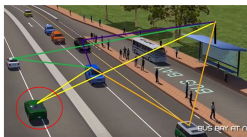
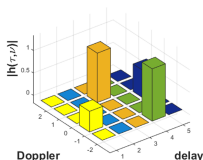
# An example: Urban multi-lane scenario



time  $t = t_0$



time  $t = t_0 + \Delta$



Example of a wireless channel in an urban multi-lane scenario illustrating the sparsity and slow variability of the channel in the DD representation.

$$y(t) = \int_{\nu} \int_{\tau} h(\tau, \nu) x(t - \tau) e^{j2\pi\nu(t - \tau)} d\tau d\nu$$

# Signal representation in delay-Doppler domain

- A signal can be represented as a function of time, or as a function of frequency, or as a quasi-periodic function of delay and Doppler
- These 3 representations are interchangeable by means of canonical transforms



$$Z_t(\phi) = \int_0^{\nu_r} e^{j2\pi t\nu} \phi(t, \nu) d\nu$$

$$Z_f(\phi) = \int_0^{\tau_r} e^{-j2\pi\tau f} \phi(\tau, f) d\tau$$

- Using **Zak transforms**  $Z_t(\phi)$  and  $Z_f(\phi)$ , symbols in DD domain can be converted into time and frequency domains

# OTFS block diagram

- Implemented using simple pre- and post-processing (ISFFT & SFFT) over any multicarrier modulation scheme such as OFDM.

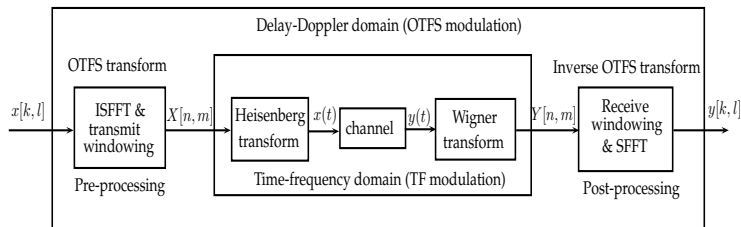


Figure : OTFS block diagram

# Signaling in delay-Doppler domain

- The information symbols in DD domain  $x[k, l]$ s are mapped to TF symbols  $X[n, m]$  using ISFFT as

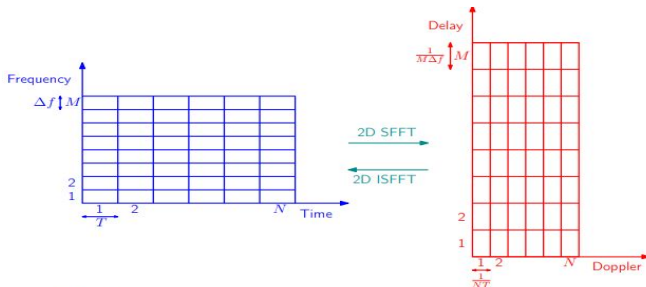
$$X[n, m] = \frac{1}{MN} \sum_{k=0}^{N-1} \sum_{l=0}^{M-1} x[k, l] e^{j2\pi \left( \frac{nk}{N} - \frac{ml}{M} \right)}$$

- TF plane is sampled at intervals  $T$  and  $\Delta f$ , to obtain a 2D grid

$$\Lambda = \{(nT, m\Delta f), n = 0, \dots, N-1, m = 0, \dots, M-1\}$$

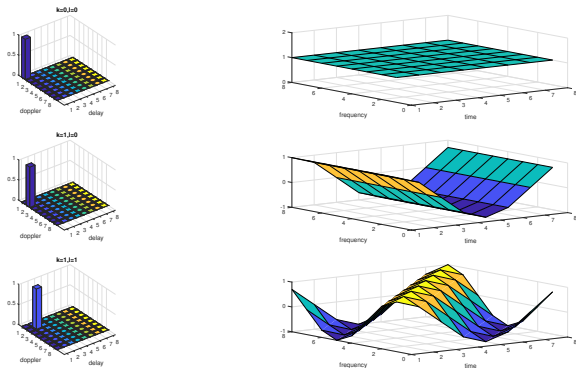
- Delay-Doppler grid  $\Gamma$ , reciprocal to  $\Lambda$

$$\Gamma = \left\{ \left( \frac{k}{NT}, \frac{l}{M\Delta f} \right), k = 0, \dots, N-1, l = 0, \dots, M-1 \right\}$$



# Signaling in delay-Doppler domain

- A 2D ISFFT translates every point on the DD plane into a corresponding basis function that covers the entire TF plane (2D orthogonal complex exponentials)



- OTFS basis functions (waveforms) have strong resilience to delay-Doppler shifts imparted by the channel (2D localized pulses in the DD domain)

# OTFS basis functions

- $M = N = 32, \Delta f = 15$  KHz

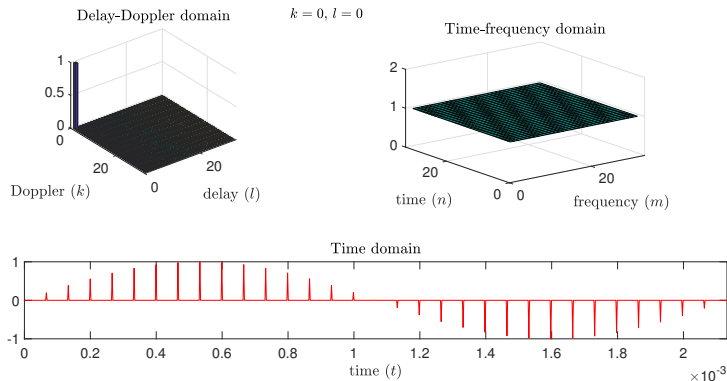


Figure : OTFS basis functions in delay-Doppler domain, time-frequency domain, and time domain for Doppler index  $k = 0$  and delay index  $l = 0$ .

# OTFS basis functions

- $M = N = 32$ ,  $\Delta f = 15$  KHz

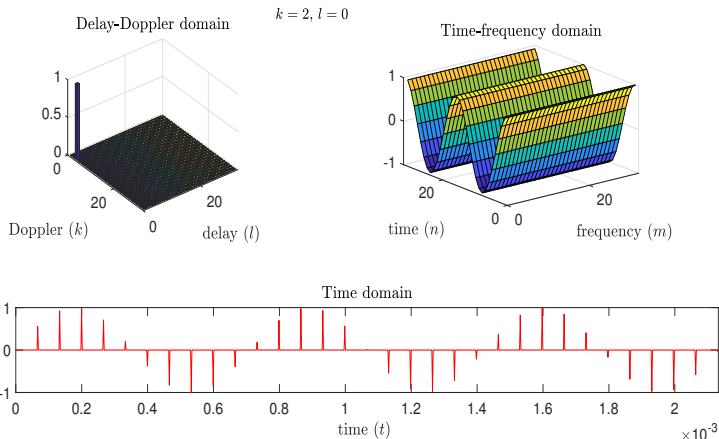


Figure : OTFS basis functions in delay-Doppler domain, time-frequency domain, and time domain for Doppler index  $k = 2$  and delay index  $l = 0$ .

# OTFS basis functions

- $M = N = 32$ ,  $\Delta f = 15$  KHz

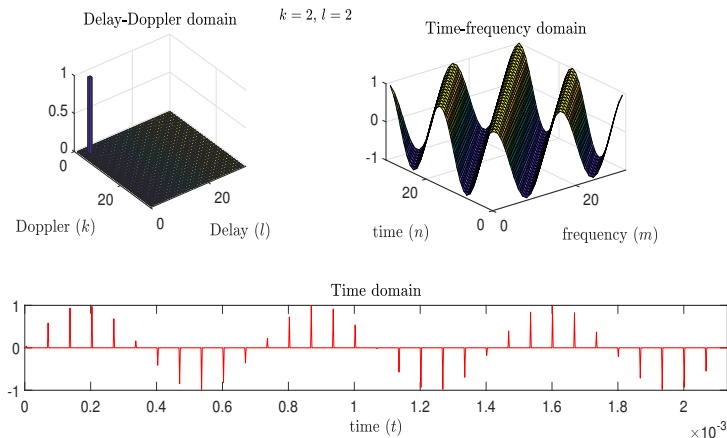


Figure : OTFS basis functions in delay-Doppler domain, time-frequency domain, and time domain for Doppler index  $k = 2$  and delay index  $l = 2$ .



# OTFS basis functions

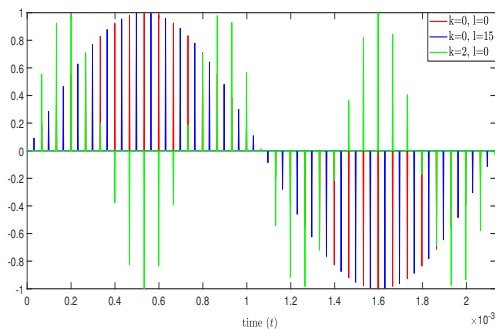


Figure : OTFS basis functions in time domain for  $(k, l) = (0, 0)$ ,  $(k, l) = (0, 15)$ , and  $(k, l) = (2, 0)$ .

- as Doppler index ( $k$ ) changes, frequency of pulse train changes (as in FDM)
- as delay index ( $l$ ) changes, position of pulses gets shifted in time (as in TDM)

# Time-frequency domain (inner block)

- **Modulator:** Heisenberg transform

$$x(t) = \sum_{n=0}^{N-1} \sum_{m=0}^{M-1} X[n, m] g_{tx}(t - nT) e^{j2\pi m \Delta f (t - nT)}$$

- **Channel:**  $h(\tau, \nu)$

$$y(t) = \int_{\nu} \int_{\tau} h(\tau, \nu) x(t - \tau) e^{j2\pi \nu (t - \tau)} d\tau d\nu$$

- **Demodulator:** Wigner Transform

$$A_{g_{rx}, y}(\tau, \nu) = \int g_{rx}^*(t - \tau) y(t) e^{-j2\pi \nu (t - \tau)} dt$$
$$Y[n, m] = A_{g_{rx}, y}(\tau, \nu) |_{\tau=nT, \nu=m\Delta f}$$

# Back to delay-Doppler domain

- If  $h(\tau, \nu)$  is bounded by  $(\tau_{\max}, \nu_{\max})$ , s.t  $\nu_{\max} < \Delta f < 1/\tau_{\max}$ , then

$$Y[n, m] = H[n, m]X[n, m] + V[n, m],$$

$$H[n, m] = \int_{\tau} \int_{\nu} h(\tau, \nu) e^{j2\pi\nu nT} e^{-j2\pi(\nu+m\Delta f)\tau} d\nu d\tau$$

- SFFT is then applied to  $Y[n, m]$  to convert it back to delay-Doppler domain to obtain  $y[k, l]$  as

$$y[k, l] = \sum_{n=0}^{N-1} \sum_{m=0}^{M-1} Y[n, m] e^{-j2\pi\left(\frac{nk}{N} - \frac{ml}{M}\right)}$$

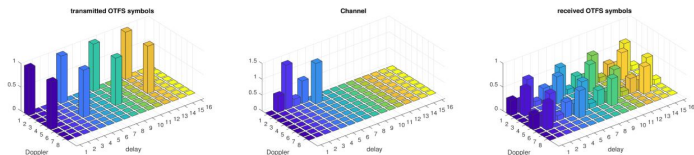
# Input-output relation

- For a channel with  $P$  paths/cluster of reflectors

$$h(\tau, \nu) = \sum_{i=1}^P h_i \delta(\tau - \tau_i) \delta(\nu - \nu_i)$$

- Received signal in delay-Doppler domain:  $\tau_i \triangleq \frac{\alpha_i}{M\Delta f}$  and  $\nu_i \triangleq \frac{\beta_i}{NT}$

$$\begin{aligned} y[k, l] &= \sum_{i=1}^P h_i e^{-j2\pi\nu_i\tau_i} x[(k - \beta_i)_N, (l - \alpha_i)_M] + v[k, l] \\ &= h[k, l] \circledast x[k, l] \quad (2D \text{ Circular Convolution}) \end{aligned}$$



- Vectorized formulation:** Input-output relation can be vectorized as

$$\mathbf{y} = \mathbf{H}\mathbf{x} + \mathbf{v},$$

where  $\mathbf{x}, \mathbf{y}, \mathbf{v} \in \mathbb{C}^{MN \times 1}$ ,  $\mathbf{H} \in \mathbb{C}^{MN \times MN}$ ,  $x_{k+NI} = x[k, l]$

# Performance of OTFS

- Simulation parameters I

Parameter	Value
Carrier frequency (GHz)	4
Subcarrier spacing (kHz)	15
Frame size ( $M, N$ )	(12, 7)
Number of paths ( $P$ )	5
Delay profile	Exponential power-delay profile
Maximum speed (km/h)	500
Modulation scheme	BPSK

- Smallest resource block used in LTE:  $M = 12, N = 7$

# OTFS performance

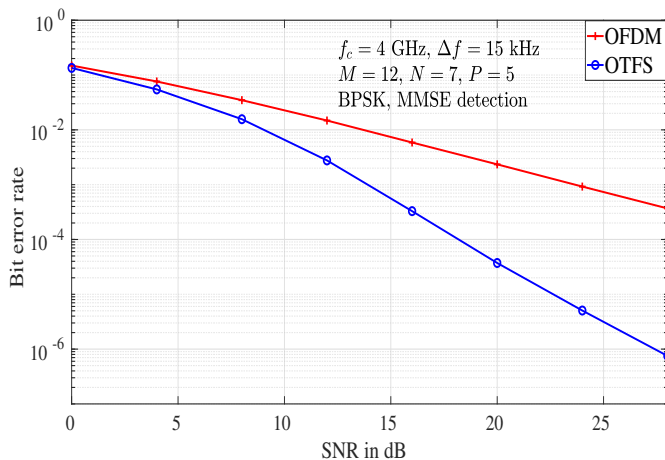


Figure : Performance of OTFS and OFDM

- Simulation parameters II: IEEE 802.11p (WAVE)

Parameter	Value
Carrier frequency (GHz)	5.9
Subcarrier spacing (MHz)	0.156
Frame size ( $M, N$ )	(64, 12)
Number of paths ( $P$ )	8
Delay profile	Exponential power-delay profile
Maximum speed (km/h)	220
Modulation scheme	BPSK



# OTFS performance

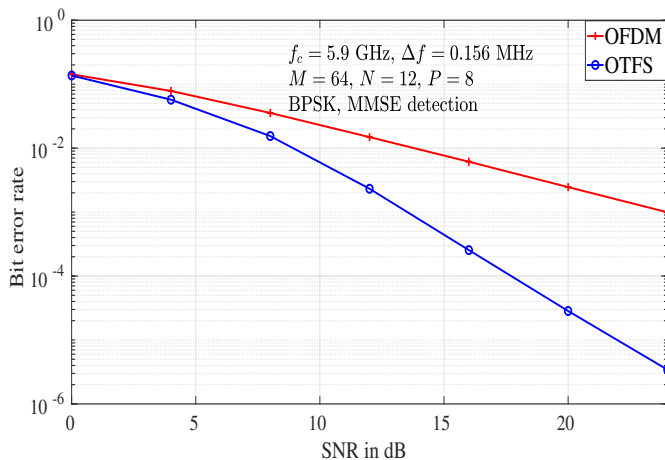


Figure : Performance of OTFS and OFDM

# Diversity in OTFS

# Diversity performance of OTFS

- There are only  $P$  non-zero elements in each row and column of the equivalent channel matrix ( $\mathbf{H}$ )
- Input-output relation can be rewritten in an alternate form as

$$\mathbf{y}^T = \mathbf{h}'\mathbf{X} + \mathbf{v}^T,$$

where  $\mathbf{h}'$  is a  $1 \times P$  vector whose  $i$ th entry is given by  $h'_i = h_i e^{-j2\pi\nu_i\tau_i}$ , and  $\mathbf{X}_{P \times MN}$  is the symbol matrix whose  $i$ th column ( $i = k + Nl$ ,  $i = 0, 1, \dots, MN - 1$ ) is given by

$$\mathbf{X}[i] = \begin{bmatrix} X(k-\beta_1)_N + N(l-\alpha_1)_M \\ X(k-\beta_2)_N + N(l-\alpha_2)_M \\ \vdots \\ X(k-\beta_P)_N + N(l-\alpha_P)_M \end{bmatrix}$$

---

(\*) G. D. Surabhi, R. M. Augustine, and A. Chockalingam, "On the diversity of uncoded OTFS modulation in doubly-dispersive channels," *IEEE Trans. Wireless Commun.*, vol. 18, no. 6, pp. 3049-3063, Jun. 2019.

# Diversity performance of OTFS

- Pairwise error probability (PEP) between  $\mathbf{X}_i$  and  $\mathbf{X}_j$

$$P(\mathbf{X}_i \rightarrow \mathbf{X}_j | \mathbf{h}', \mathbf{X}_i) = Q \left( \sqrt{\frac{\|\mathbf{h}'(\mathbf{X}_i - \mathbf{X}_j)\|^2}{2N_0}} \right)$$

- PEP averaged over the channel statistics can be upper bounded as

$$P(\mathbf{X}_i \rightarrow \mathbf{X}_j) \leq \frac{1}{\gamma^r \prod_{l=1}^r \frac{\lambda_l^2}{4P}}$$

where  $\lambda_l$  is the  $l$ th non-zero singular value of the difference matrix  $\mathbf{\Delta}_{ij} = (\mathbf{X}_i - \mathbf{X}_j)$ ,  $r$  is the rank of  $\mathbf{\Delta}_{ij}$ , and  $\gamma$  is the SNR

- Diversity order

$$\rho_{\text{siso-otfs}} = \min_{i, j, i \neq j} \text{rank}(\mathbf{\Delta}_{ij})$$

which is **one**

# Lower bound on BER

- BER can be bounded as

$$\text{BER} \geq \frac{1}{2^{MN}} \sum_{k=1}^{\kappa} P(\mathbf{X}_i \rightarrow \mathbf{X}_j),$$

where  $\kappa$  denotes the number of  $\mathbf{\Delta}_{ij}$ s having rank one

- Assuming BPSK symbols,

$$P(\mathbf{X}_i \rightarrow \mathbf{X}_j) = \mathbb{E} \left[ Q \left( \sqrt{2\gamma PMN |\tilde{h}_1|^2} \right) \right]$$

- At high SNRs,

$$\text{BER} \geq \frac{\kappa}{2^{MN}} \frac{1}{4\gamma MN}$$

- As the values  $M$  and  $N$  increase, the  $2^{MN}$  term can dominate the ratio  $\frac{\kappa}{2^{MN}}$
- BER can decrease with a higher slope for higher frame sizes before meeting the diversity one lower bound

---

<sup>1</sup>When  $P = MN$ ,  $\kappa = 8 \forall MN$

# Diversity results

Simulation parameters:

Parameter	Value
Carrier frequency (GHz)	4
Subcarrier spacing (kHz)	3.75
Number of paths ( $P$ )	4
Delay-Doppler profile ( $\tau_j, \nu_j$ )	$(0, 0), (0, \frac{1}{NT}), (\frac{1}{M\Delta f}, 0), (\frac{1}{M\Delta f}, \frac{1}{NT})$
Modulation scheme	BPSK

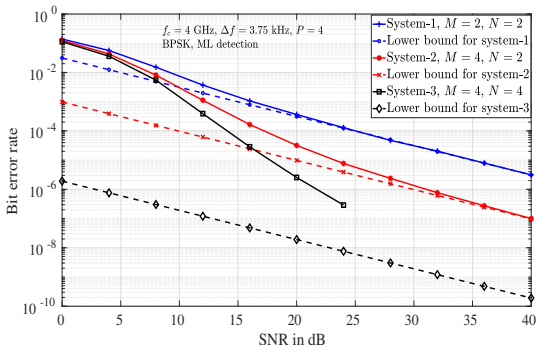


Figure : BER performance of OTFS for *i*)  $M = 2, N = 2$ , *ii*)  $M = 4, N = 2$ , *iii*)  $M = 4, N = 4$ .

# Effect of frame size

- Note that the  $\frac{\kappa}{2^{MN}}$  values for the considered systems are  $\frac{8}{16}$ ,  $\frac{8}{256}$ , and  $\frac{8}{65536}$ , respectively.
- Though the asymptotic diversity order is one, increasing the frame size can lead to higher slopes ( $> 1$ ) for BER curves in the finite SNR regime.

## Choice of M & N

- M decides the delay resolution and  $\nu_{\max} < \frac{B}{M} = \Delta f < 1/\tau_{\max}$ .
- N decides Doppler resolution and latency ( $T_l = NT$ ).
- Example: For  $\tau_{\max} = 1 \mu\text{s}$ ,  $\nu_{\max} = 5 \text{ kHz}$ ,  $B = 10 \text{ MHz}$ , and  $T_l = 1 \text{ ms}$ ,
  - $\nu_{\max} < \Delta f < 1/\tau_{\max} \implies 5 \text{ KHz} < \Delta f < 1 \text{ MHz}$
  - $\Delta f$  can be chosen to be 20 kHz ( $\implies M = \frac{10 \times 10^6}{20 \times 10^3} = 500$ )
  - $T_l = NT = \frac{N}{\Delta f}$ ;  $\implies N = T_l \Delta f = 1 \times 10^{-3} \times 20 \times 10^3 = 20$
  - $(M, N)$  can be chosen as (500,20)

# Phase rotation for full diversity

- Let

$$\mathbf{\Phi} = \text{diag} \left\{ \phi_0^{(0)}, \dots, \phi_{N-1}^{(0)}, \phi_0^{(1)}, \dots, \phi_{N-1}^{(1)}, \dots, \phi_{N-1}^{(M-1)} \right\}$$

be the phase rotation matrix and

$$\mathbf{x}' = \mathbf{\Phi} \mathbf{x}$$

be the phase rotated OTFS transmit vector.

- OTFS with the above phase rotation achieves the full diversity of  $P$  when  $\phi_q^{(l)} = e^{ja_q^{(l)}}$ ,  $q = 0, \dots, N-1$ ,  $l = 0, \dots, M-1$  are transcendental numbers with  $a_q^{(l)}$  real, distinct, and algebraic.



# Full diversity using phase rotation

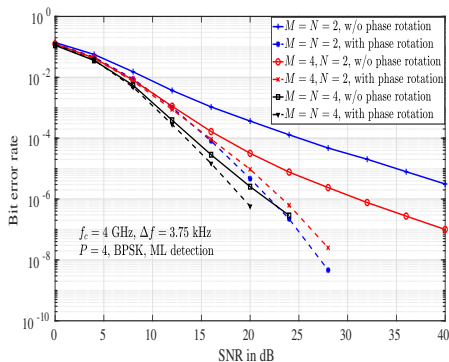


Figure : BER performance of OTFS without and with phase rotation for *i*)  $M = N = 2$ , *ii*)  $M = 4, N = 2$ , and *iii*)  $M = N = 4$ , and BPSK.

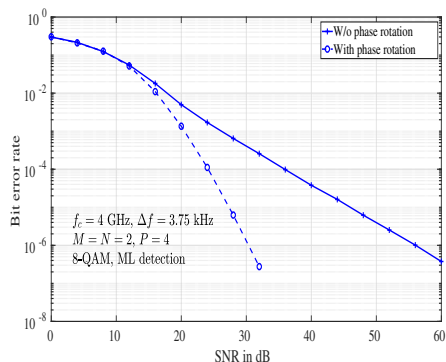


Figure : BER performance of OTFS without and with phase rotation,  $M = N = 2$ , and 8-QAM.

$${}^1\Phi = \text{diag}\{1, e^{j\frac{1}{MN}} \dots e^{j\frac{MN-1}{MN}}\}$$

# MIMO-OTFS

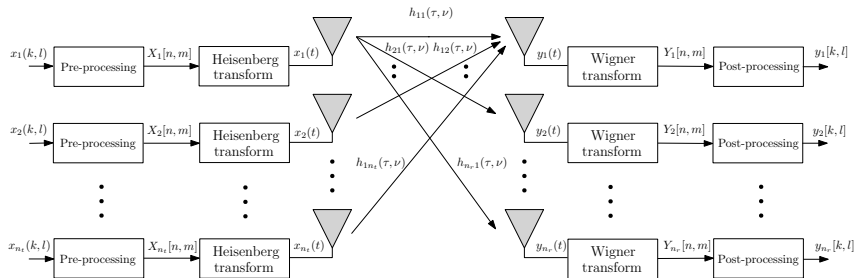


Figure : Block diagram of MIMO-OTFS scheme

$$\mathbf{y}_{\text{MIMO}} = \mathbf{H}_{\text{MIMO}} \mathbf{x}_{\text{MIMO}} + \mathbf{v}_{\text{MIMO}}$$

(\*) M. K. Ramachandran and A. Chockalingam, "MIMO-OTFS in high-Doppler fading channels: Signal detection and channel estimation," *Proc. IEEE GLOBECOM'2018*, Abu Dhabi, UAE, Dec. 2018.

# MIMO-OTFS performance

- Delay and Doppler models

Path index ( $i$ )	1	2	3	4	5
Delay ( $\tau_i, \mu\text{s}$ )	2.1	4.2	6.3	8.4	10.4
Doppler ( $\nu_i, \text{Hz}$ )	0	470	940	1410	1880

- Simulation parameters

Parameter	Value
Carrier frequency (GHz)	4
Subcarrier spacing (kHz)	15
Frame size ( $M, N$ )	(32, 32)
Modulation scheme	BPSK
MIMO configuration	$1 \times 1$ , $1 \times 2$ , $1 \times 3$ , $2 \times 2$ , $3 \times 3$ , $2 \times 3$
Maximum speed (kmph)	507.6

# MIMO-OTFS performance

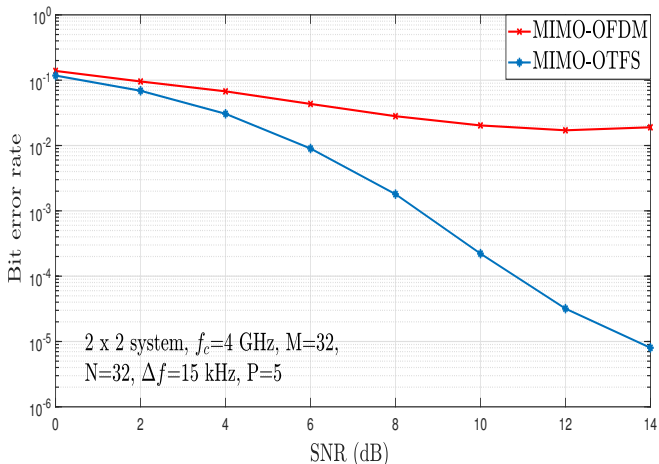


Figure : BER performance comparison between MIMO-OTFS and MIMO-OFDM

# Diversity of MIMO-OTFS

- Each row of  $\mathbf{H}_{\text{MIMO}}$  has only  $n_t P$  non-zero elements and each column has only  $n_r P$  non-zero elements. The MIMO-OTFS system model can be written as

$$\begin{bmatrix} \mathbf{y}_1^T \\ \mathbf{y}_2^T \\ \vdots \\ \mathbf{y}_{n_r}^T \end{bmatrix} = \begin{bmatrix} \mathbf{h}'_{11} & \mathbf{h}'_{12} & \cdots & \mathbf{h}'_{1n_t} \\ \mathbf{h}'_{21} & \mathbf{h}'_{22} & \cdots & \mathbf{h}'_{2n_t} \\ \vdots & \vdots & \ddots & \vdots \\ \mathbf{h}'_{n_r 1} & \mathbf{h}'_{n_r 2} & \cdots & \mathbf{h}'_{n_r n_t} \end{bmatrix} \begin{bmatrix} \mathbf{X}_1 \\ \mathbf{X}_2 \\ \vdots \\ \mathbf{X}_{n_t} \end{bmatrix} + \begin{bmatrix} \mathbf{v}_1^T \\ \mathbf{v}_2^T \\ \vdots \\ \mathbf{v}_{n_r}^T \end{bmatrix},$$

- Diversity order achieved by MIMO-OTFS can be derived as

$$\rho_{\text{mimo-otfs}} = n_r \cdot \min_{i,j} \text{rank}(\Delta_{k,ij}) = n_r$$

- If  $MN \times 1$  OTFS transmit vector from each antenna is multiplied by the phase rotation matrix  $\Phi$ , then diversity order achieved by phase rotated MIMO-OTFS system is equal to  $Pn_r$

# Diversity results in MIMO-OTFS

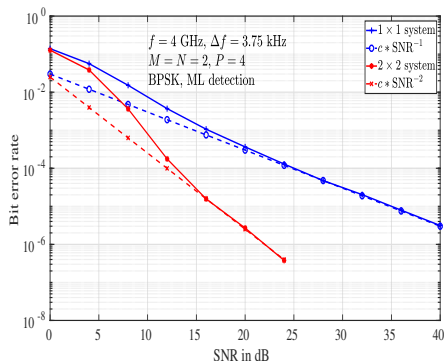


Figure : BER performance of  $1 \times 1$  SISO-OTFS and  $2 \times 2$  MIMO-OTFS systems.

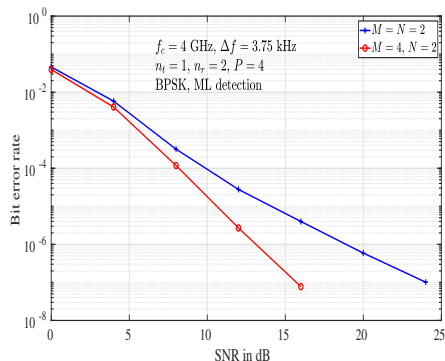


Figure : BER performance of  $1 \times 2$  OTFS system with  $i)$   $M = N = 2$  and  $ii)$   $M = 4, N = 2$ .

# Full diversity using phase rotation in MIMO-OTFS

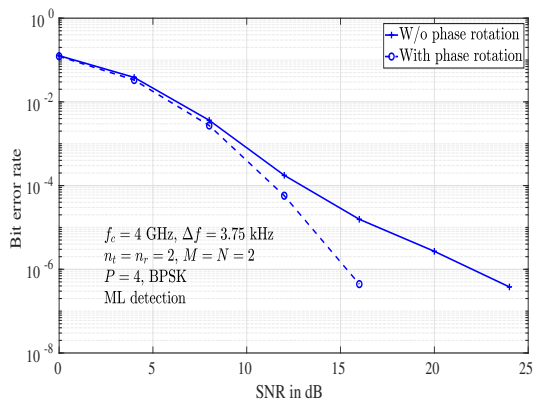


Figure : BER performance of  $2 \times 2$  MIMO-OTFS system without and with phase rotation,  $M = N = 2$ .



# Space-time coded OTFS

# Space-time coded OTFS

- Use of space-time coding in OTFS
- structure of Alamouti code generalized to matrices

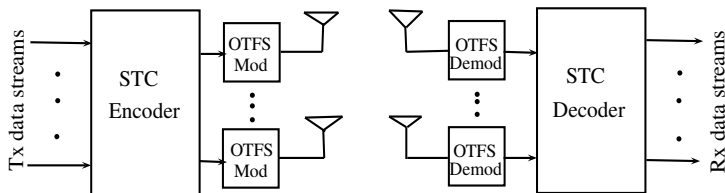


Figure : STC-OTFS scheme.

- Consider the alternate form of input-output relation for SISO-OTFS

$$\mathbf{y}^T = \mathbf{h}'\mathbf{X} + \mathbf{v}^T,$$

where  $\mathbf{X}$  is an  $MN \times MN$  symbol matrix.

---

(\*) Rose Mary Augustine, G. D.Surabhi and A. Chockalingam, "Space-time coded OTFS modulation in high-Doppler channels," *Proc. IEEE VTC'2019-Spring*, Kuala Lumpur Apr. 2019.

# Encoding

- Consider a space-time code (rate-1) using the Alamouti code structure (generalized to matrices)
- quasi-static DD channel over  $T' (= 2)$  frames

$$\tilde{\mathbf{X}}_{n_t MN \times T' MN} = \tilde{\mathbf{X}}_{2MN \times 2MN} = \begin{bmatrix} \mathbf{X}_1 & -\mathbf{X}_2^H \\ \mathbf{X}_2 & \mathbf{X}_1^H \end{bmatrix}$$

- Corresponding OTFS transmit vectors,  $k \in \{1, 2\}$

$$\mathbf{X}_k \iff \mathbf{x}_k, \quad \mathbf{X}_k^H \iff (\hat{\mathbf{x}}_k)^* = (\mathbf{P}\mathbf{x}_k)^*.$$

where

$$\mathbf{P} = \mathbf{P}'_M \otimes \mathbf{P}'_N.$$

$$\mathbf{P}'_M = \begin{bmatrix} 1 & 0 & \cdots & 0 & 0 \\ 0 & 0 & \cdots & 0 & 1 \\ 0 & 0 & \cdots & 1 & 0 \\ \vdots & & & & \\ 0 & 1 & \cdots & 0 & 0 \end{bmatrix}_{M \times M}, \quad \mathbf{P}'_N = \begin{bmatrix} 1 & 0 & \cdots & 0 & 0 \\ 0 & 0 & \cdots & 0 & 1 \\ 0 & 0 & \cdots & 1 & 0 \\ \vdots & & & & \\ 0 & 1 & \cdots & 0 & 0 \end{bmatrix}_{N \times N}.$$

- Transmitted OTFS vectors in the second frame duration are not just the conjugated vectors, but are conjugated and permuted vectors of those transmitted in the first frame duration.

- Received vectors in the first and second frame duration are

$$\begin{aligned}\mathbf{y}_1 &= \mathbf{H}_1 \mathbf{x}_1 + \mathbf{H}_2 \mathbf{x}_2 + \mathbf{v}_1 \\ \mathbf{y}_2 &= -\mathbf{H}_1(\hat{\mathbf{x}}_2)^* + \mathbf{H}_2(\hat{\mathbf{x}}_1)^* + \mathbf{v}_2.\end{aligned}$$

- Permutation ( $\mathbf{P}$ ) and conjugation are applied on  $\mathbf{y}_2$ .

$$\underbrace{\begin{bmatrix} \mathbf{y}_1 \\ (\hat{\mathbf{y}}_2)^* \end{bmatrix}}_{\triangleq \bar{\mathbf{y}}} = \underbrace{\begin{bmatrix} \mathbf{H}_1 & \mathbf{H}_2 \\ \mathbf{H}_2^H & -\mathbf{H}_1^H \end{bmatrix}}_{\triangleq \bar{\mathbf{H}}} \begin{bmatrix} \mathbf{x}_1 \\ \mathbf{x}_2 \end{bmatrix} + \begin{bmatrix} \mathbf{v}_1 \\ (\hat{\mathbf{v}}_2)^* \end{bmatrix}$$

- Since two block columns of  $\bar{\mathbf{H}}$  are orthogonal, the decoding problem for  $\mathbf{x}_1$  and  $\mathbf{x}_2$  can be decomposed into two separate orthogonal problems.

- Let  $\tilde{\mathbf{\Delta}}_{ij} \triangleq \tilde{\mathbf{X}}_i - \tilde{\mathbf{X}}_j$  be the difference matrix

$$\rho_{\text{STC-OTFS}} = \min\left\{\min_{i,j, i \neq j} \text{rank}(\tilde{\mathbf{\Delta}}_{ij}), 2P\right\}.$$

- $\text{rank}(\tilde{\mathbf{\Delta}}_{ij})$  can be simplified as

$$\text{rank}(\tilde{\mathbf{\Delta}}_{ij}^H \tilde{\mathbf{\Delta}}_{ij}) = 2 \times \text{rank}(\mathbf{\Delta}_{1,ij}^H \mathbf{\Delta}_{1,ij} + \mathbf{\Delta}_{2,ij}^H \mathbf{\Delta}_{2,ij}).$$

whose min rank is **two**.

- STC-OTFS for  $2 \times n_r$  can achieve an asymptotic diversity order of  $2n_r$ .
- With phase rotation applied to each of  $n_t$  transmit antennas during every frame duration can yield a **full delay Doppler space diversity of  $2Pn_r$** .

# BER performance of STC-OTFS

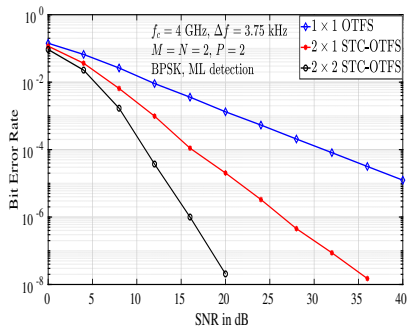


Figure : BER performance of *i*)  $1 \times 1$  OTFS, *ii*)  $2 \times 1$  STC-OTFS, and *iii*)  $2 \times 2$  STC-OTFS for  $M = N = 2$ .

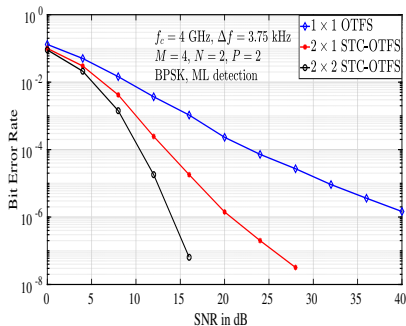


Figure : BER performance of *i*)  $1 \times 1$  OTFS, *ii*)  $2 \times 1$  STC-OTFS, and *iii*)  $2 \times 2$  STC-OTFS for  $M = 4, N = 2$ .

# Phase rotation in STC-OTFS

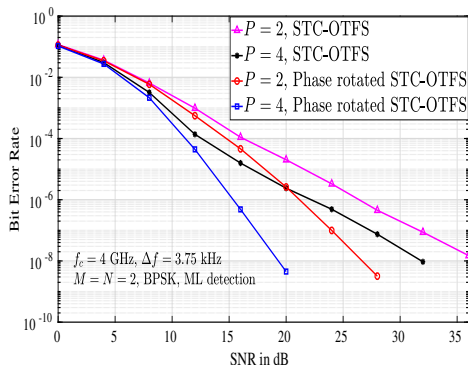


Figure : BER performance of  $2 \times 1$  STC-OTFS with and without phase rotation for *i*)  $P = 2$  and *ii*)  $P = 4$ .

STC-OTFS with phase rotation achieves **full spatial and delay-Doppler diversity** even for small frame sizes.

# PAPR of OTFS



- High PAPR is one of the key detrimental aspects in OFDM systems
  - Max. PAPR in OFDM increases with  $M$ , no. of subcarriers due to  $M$ -point IDFT operation at transmitter

## PAPR of OTFS waveform is of interest

- In OTFS, max. PAPR grows linearly with  $N$  (and not with  $M$ )

---

(\*) G. D. Surabhi, R. M. Augustine and A. Chockalingam, "Peak-to-average power ratio of OTFS modulation," *IEEE Commun. Letters*, vol. 23, no. 6, pp. 999-1002, Jun. 2019.

(\*\*) S. Tiwari and S. S. Das, "Circularly pulse shaped orthogonal time frequency space modulation," arXiv:1910.10457v1 [cs.IT] 23 Oct 2019.

# PAPR of OTFS transmit signal

- Time domain OTFS signal is given by

$$s(t) = \sum_{n=0}^{N-1} \sum_{m=0}^{M-1} X[n, m] g_{tx}(t - nT) e^{j2\pi m \Delta f (t - nT)}$$

- Discrete time representation (by Nyquist sampling,  $t = (r + qM)T_s$ ):

$$s(r + qM) = M \sum_{n=0}^{N-1} \tilde{x}_r[n] g_{tx}([r + qM - nM]_{MN})$$

where  $\tilde{x}_r[n] = \sum_{k=0}^{N-1} x[k, r] e^{\frac{j2\pi nk}{N}}$  ( $n$ th IDFT),  $r = 0, \dots, M - 1$  and  $q = 0, \dots, N - 1$

# Upper bound on PAPR

$$\text{PAPR} = \frac{\max_{r,q} \{|s(r + qM)|^2\}}{P_{\text{avg}}},$$

where

$$P_{\text{avg}} = \frac{M^2 N \sigma_a^2}{MN} \sum_{n=0}^{N-1} \sum_{r=0}^{M-1} \sum_{q=0}^{N-1} |g_{\text{tx}}([r + qM - nM]_{MN})|^2$$

$$\max_{r,q} |s(r + qM)|^2 \leq M^2 N^2 \max_{k,l} |x[k, l]|^2 \max_{r,q} \sum_{n=0}^{N-1} |g_{\text{tx}}([r + qM - nM]_{MN})|^2$$

For rectangular pulse,

$$\text{PAPR}_{\text{max}} = \frac{N \max_{c \in \mathbb{A}} |c|^2}{\sigma_a^2}$$

**PAPR<sub>max</sub> grows linearly with  $N$  and not with  $M$ .**

- Time domain samples of the OTFS transmit signal with rectangular pulse are the  $N$ -point IDFT values of the DD symbols along Doppler domain.
- If  $N$  is large, then by CLT, the transmitted samples can be approximated to have complex Gaussian distribution with zero mean.
- CCDF of PAPR can be derived as

$$P(\text{PAPR} > \gamma_0) \approx 1 - (1 - e^{-\gamma_0})^{MN}$$

# PAPR performance of OTFS

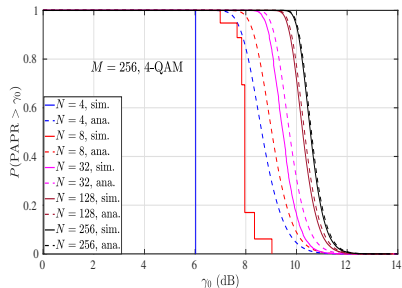


Figure : Analytical and simulated CCDF of PAPR in OTFS.

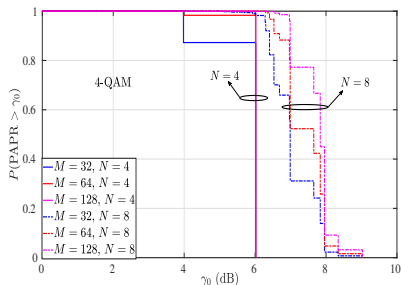


Figure : Effect of  $M$  and  $N$  on the CCDF of PAPR in OTFS.

# PAPR of OTFS, OFDM and GFDM

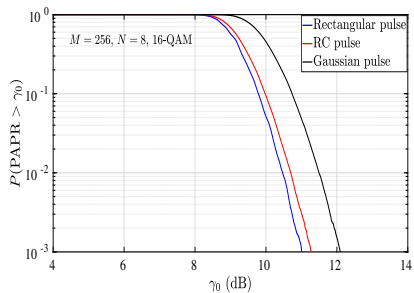


Figure : CCDF of the PAPR of OTFS for different pulse shapes.

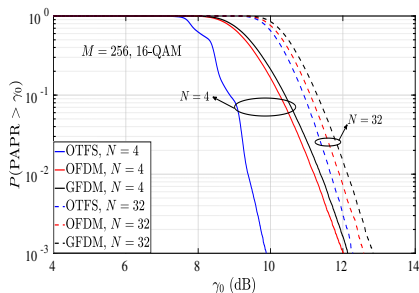


Figure : Comparison of CCDF of the PAPR of OTFS with those of OFDM and GFDM with 16-QAM.

OTFS can have better PAPR compared to OFDM and GFDM when  $N < M$ .

# Channel estimation in OTFS

# Channel estimation in the delay-Doppler domain

- Each tx and rx antenna pair sees a different channel having a finite support in the delay-Doppler domain
- The support is determined by the delay and Doppler spread of the channel
- Input-output relation for  $p$ th tx and  $q$ th rx antenna pair can be written as

$$\hat{x}_q[k, l] = \sum_{m=0}^{M-1} \sum_{n=0}^{N-1} x_p[n, m] \frac{1}{MN} h_{w_{qp}} \left( \frac{k-n}{NT}, \frac{l-m}{M\Delta f} \right) + v_q[k, l]$$

- Transmit pilot from  $p$ th antenna

$$\begin{aligned} x_p[n, m] &= 1 \text{ if } (n, m) = (n_p, m_p) \\ &= 0 \quad \forall (n, m) \neq (n_p, m_p) \end{aligned}$$

- Received signal at the  $q$ th rx antenna will be

$$\hat{x}_q[k, l] = \frac{1}{MN} h_{w_{qp}} \left( \frac{k-n_p}{NT}, \frac{l-m_p}{M\Delta f} \right) + v_q[k, l]$$

- $\frac{1}{MN} h_{w_{qp}} \left( \frac{k}{NT}, \frac{l}{M\Delta f} \right)$  and thus  $\hat{\mathbf{H}}_{qp}$  can be estimated, since  $n_p$  and  $m_p$  are known at the receiver a priori



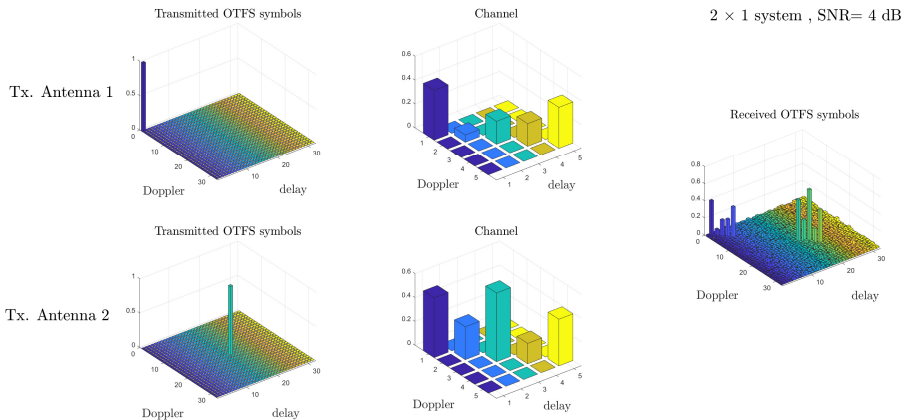


**Figure :** Illustration of pilots and channel response in delay-Doppler domain in a  $2 \times 1$  MIMO-OTFS system

# MIMO-OTFS performance with the estimated channel

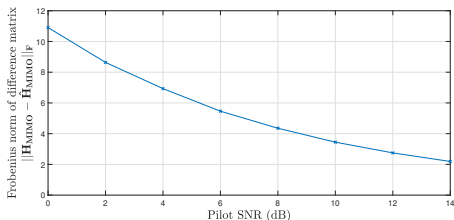


Figure : Frobenius norm of the difference matrix  $\mathbf{H}_{\text{MIMO}} - \hat{\mathbf{H}}_{\text{MIMO}}$  as a function of pilot SNR in a  $2 \times 2$  MIMO-OTFS system

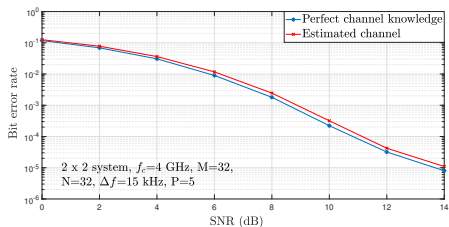
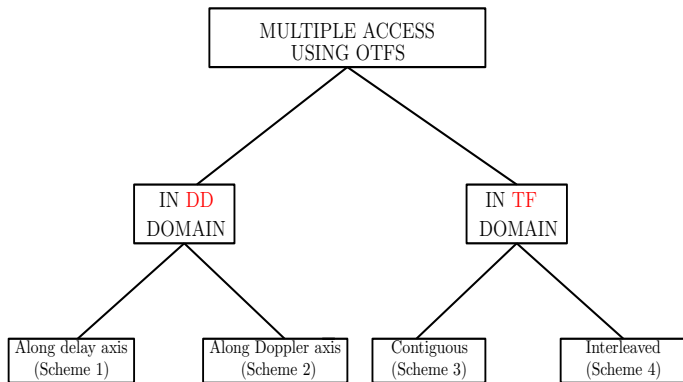


Figure : BER performance of  $2 \times 2$  MIMO-OTFS system using the estimated channel

# Multiuser OTFS (OTFS-MA)

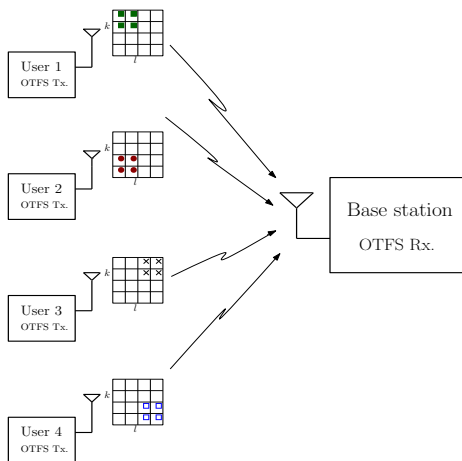


(\*) G. D. Surabhi, R. M. Augustine, and A. Chockalingam, "Multiple access in the delay-Doppler domain using OTFS modulation," *ITA'2019*, San Diego, Feb. 2019. Online: arXiv:1902.03415 [sc.IT] 9 Feb 2019.

(\*\*) V. Khammammetti and S. K. Mohammed, "OTFS based multiple-access in high Doppler and delay spread wireless channels," *IEEE Wireless Commun. Lett.*, doi: 10.1109/LWC.2018.2878740.

(\*\*\*) R. M. Augustine and A. Chockalingam, "Interleaved time-frequency multiple access using OTFS modulation," *IEEE VTC2019-Fall*, Honolulu, Sep. 2019.

# OTFS-MA in the delay-Doppler domain



- Bins in the delay-Doppler grid  $\Gamma$  serve as the delay-Doppler resource blocks (DDRBs)
- Different DDRBs are allocated to different users for multiple access
- Denoting the OTFS symbol vector transmitted by  $u$ th user by  $\mathbf{x}_u \in \mathbb{C}^{MN \times 1}$

$$\mathbf{y} = \sum_{u=0}^{K_u-1} \mathbf{H}_u \mathbf{x}_u + \mathbf{v}$$

Figure : OTFS multiple access (OTFS-MA) on the uplink

# DDRB allocation schemes

Scheme 1- Multiplexing along delay axis

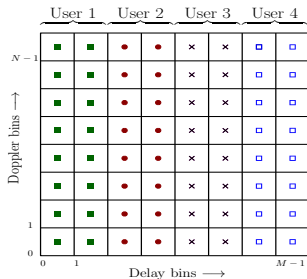


Figure : DDRB allocation in an  $N \times M$  delay-Doppler grid in Scheme 1.

Scheme 2- Multiplexing along Doppler axis

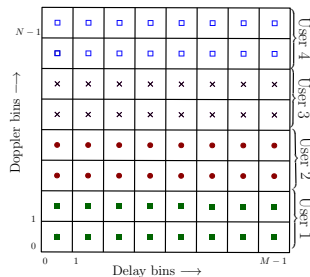


Figure : DDRB allocation in an  $N \times M$  delay-Doppler grid in Scheme 2.

The 2D circular convolution operation with channel results in each user's symbols to experience MUI, requiring the BS to jointly decode the symbols.

# DDRB allocation schemes

## Scheme 3 - MUI-free allocation

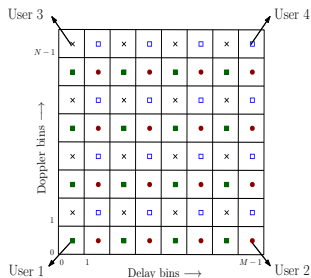


Figure : DDRB allocation in an  $N \times M$  delay-Doppler grid in Scheme 3 .

- $MN/K_u$  symbols from a given user are placed at equal intervals in the delay as well as Doppler domains ( $g_1$  and  $g_2$  respectively where  $K_u = g_1 g_2$ ) .
- $X_u[n, m]$  can be restricted to a region  $[\frac{NT}{g_2}(u)_{g_2}, \frac{NT}{g_2}((u)_{g_2} + 1)]$  in time and  $[\frac{M}{g_1} \lfloor u/g_2 \rfloor \Delta f, \frac{M}{g_1} (\lfloor u/g_2 \rfloor + 1) \Delta f]$  in frequency.
- Reduced detection complexity.

<sup>1</sup>V. Khammammetti, S. K. Mohammed, "OTFS based multiple-access in high Doppler and delay spread wireless channels," *IEEE Wireless Commun. Lett.* vol. 8, pp. 528-531, Apr. 2019.

# OTFS-MA performance

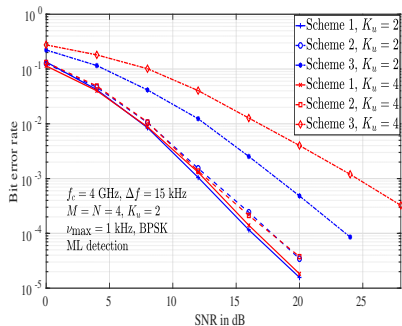


Figure : BER performance of uplink OTFS-MA with different DDRB allocation schemes with  $M = N = 4$ ,  $K_u = 2, 4$ , and ML detection<sup>1</sup>.

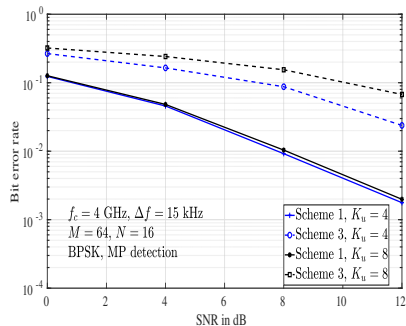


Figure : BER performance of uplink OTFS-MA with DDRB allocation Schemes 1 and 3 with  $K_u = 4, 8$  users,  $M = 64$ ,  $N = 16$ , and MP detection<sup>2</sup>

<sup>1</sup> 4 tap channel,  $\tau_{u,i} = \{0, 16.6, 33.3, 50\} \mu s$ ,  $\nu_{\max} = 1$  KHz  $\forall u$

<sup>2</sup> 10 tap channel,  $\tau_{u,i} = \{0, 1.04, 2.08, 3.12, 4.16, 5.2, 6.25, 7.29, 8.33, 9.37\} \mu s$ ,  $\nu_{\max} = 1$  KHz  $\forall u$ .



# OTFS-MA Vs SC-FDMA and OFDMA

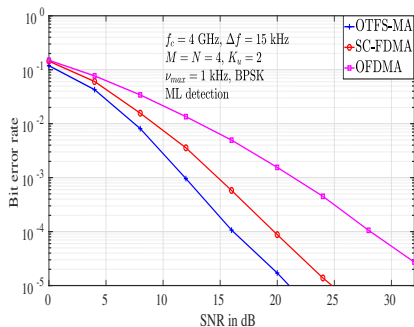


Figure : BER performance comparison between OTFS-MA, OFDMA, and SC-FDMA with ML detection.

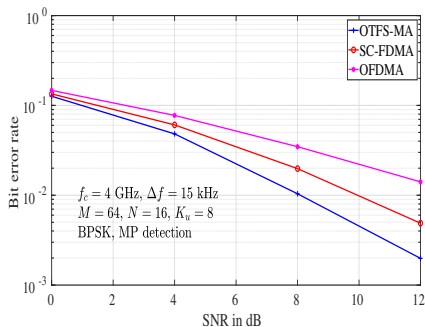


Figure : BER performance comparison between OTFS-MA, OFDMA, and SC-FDMA with MP detection.

- OTFS-MA achieves better performance compared to OFDMA and SC-FDMA on the uplink.

# OTFS with phase noise

# OTFS with phase noise

- Phase noise spectrum

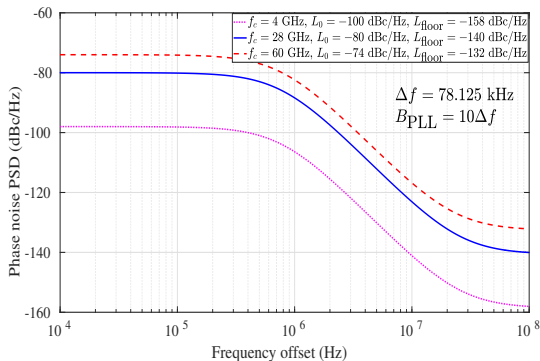


Figure : PSD of oscillator phase noise for various carrier frequencies (4 GHz, 28 GHz, 60 GHz).

$$L(f_m) = \frac{B_{\text{PLL}}^2 L_0}{B_{\text{PLL}}^2 + f_m^2} + L_{\text{floor}}$$

(\*) G. D. Surabhi, M. K. Ramachandran, and A. Chockalingam, "OTFS modulation with phase noise in mmWave communications," *Proc. IEEE VTC'2019-Spring*, Kuala Lumpur, Apr. 2019.

# PLL bandwidth and variance of phase noise

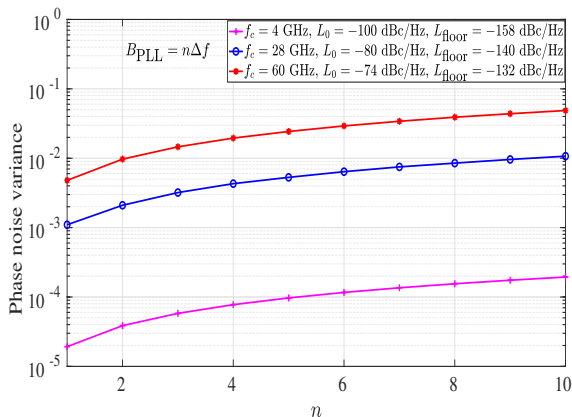


Figure : Variance of the oscillator phase noise as a function of  $n$  where  $B_{\text{PLL}} = n\Delta f$ .

# Simulation parameters

Parameter	Value
Carrier frequency (GHz)	28
Bandwidth (MHz)	10
Subcarrier spacing, $\Delta f$ (kHz)	78.125
Frame size ( $M, N$ )	(128,64)
Modulation	BPSK
No. of taps, $P$	5
Delay profile ( $\mu\text{s}$ )	0.3, 1, 1.7, 2.4, 3.1
Doppler profile (Hz)	0, -400, 400, -1220, 1220

# BER performance

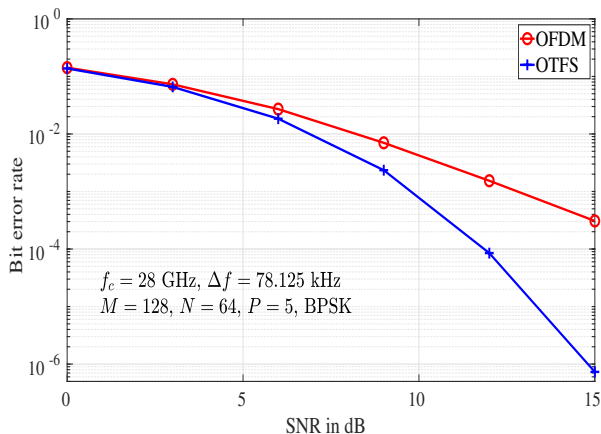


Figure : BER performance comparison between OTFS and OFDM systems with phase noise and Doppler shifts.

- OTFS modulation
  - an emerging and promising modulation scheme for high-Doppler fading channels
  - multiplexing in the delay-Doppler domain
  - impressive performance (superior performance compared to OFDM)
  - implementation using pre- and post-processing blocks to OFDM
  - simple channel estimation in the delay-Doppler domain
  - can serve in interesting use cases (high-speed trains, autonomous vehicles, drones, mmWave communications)
  - Promising modulation scheme for 5G and beyond

# Publications from our group

- G. D. Surabhi and A. Chockalingam, "Low-complexity Linear Equalization for OTFS modulation," *IEEE Commun. Letters*, Nov. 2019.
- G. D. Surabhi, R. M. Augustine, and A. Chockalingam, "On the diversity of uncoded OTFS modulation in doubly-dispersive channels," *IEEE Trans. Wireless Commun.*, vol. 18, no. 6, pp. 3049-3063, Jun. 2019.
- G. D. Surabhi, R. M. Augustine and A. Chockalingam, "Peak-to-average power ratio of OTFS modulation," *IEEE Commun. Letters*, vol. 23, no. 6, pp. 999-1002, Jun. 2019.
- R. M. Augustine and A. Chockalingam, "Interleaved time-frequency multiple access using OTFS modulation," *IEEE VTC2019-Fall*, Honolulu, Sep. 2019.
- G. D. Surabhi, R. M. Augustine, and A. Chockalingam, "Multiple access in the delay-Doppler domain using OTFS modulation," *ITA'2019*, San Diego, Feb. 2019. Online: arXiv:1902.03415 [cs.IT] 9 Feb 2019.
- Rose Mary Augustine, G. D.Surabhi and A. Chockalingam, "Space-time coded OTFS modulation in high-Doppler channels," *Proc. IEEE VTC'2019-Spring*, Kuala Lumpur Apr. 2019.
- G. D. Surabhi, M. K. Ramachandran, and A. Chockalingam, "OTFS modulation with phase noise in mmWave communications," *Proc. IEEE VTC'2019-Spring*, Kuala Lumpur Apr. 2019.
- M. K. Ramachandran and A. Chockalingam, "MIMO-OTFS in high-Doppler fading channels: Signal detection and channel estimation," *Proc. IEEE GLOBECOM'2018*, Abu Dhabi, UAE, Dec. 2018. Online: arXiv:1805.02209 [cs.IT] 6 May 2018.
- K. R. Murali and A. Chockalingam, "On OTFS modulation for high-Doppler fading channels," *ITA'2018*, San Diego, Feb. 2018. Online: arXiv:1802.00929 [cs.IT] 3 Feb 2018.



**Thank you**